Nuclear structure model for double-charge-exchange processes

V. dos S. Ferreira,[1] A. R. Samana,[2,*] F. Krmpotić,[3] and M. Chiapparini[1]

[1]*Instituto de Física, Universidade do Estado do Rio de Janeiro, CEP 20550-900, Rio de Janeiro-RJ, Brazil*

[2]*Departamento de Ciências Exactas e Tecnológicas, Universidade Estadual de Santa Cruz, CEP 45662-000 Ilhéus, Bahia-BA, Brazil*

[3]*Instituto de Física La Plata, CONICET, Universidad Nacional de La Plata, 1900 La Plata, Argentina*

(Received 23 October 2019; revised manuscript received 3 February 2020; accepted 27 February 2020; published 21 April 2020)

A new model, based on the BCS approach, is especially designed to describe nuclear phenomena $(A, Z) \rightarrow (A, Z \pm 2)$ of double-charge exchange (DCE). Although it was proposed and applied in the particle-hole limit, by one of the authors [Krmpotić, Fizika B **14**, 139 (2005)], it has not yet been applied within the BCS mean-field framework, nor has its ability to describe DCE processes been thoroughly explored. It is a natural extension of the *pn*-QRPA model, developed by Halbleib and Sorensen [Nucl. Phys. A **98**, 542 (1967)] to describe the single β decays $(A, Z) \rightarrow (A, Z \pm 1)$, to the DCE processes. As such, it exhibits several advantages over the *pn*-QRPA model when used in the evaluation of the double beta decay (DBD) rates. For instance, (i) the extreme sensitivity of the nuclear matrix elements (NMEs) on the model parametrization does not occur; (ii) it allows us to study the NMEs, not only for the ground state in daughter nuclei, as the *pn*-QRPA model does, but also for all final 0^+ and 2^+ states, accounting at the same time for their excitation energies and the corresponding DBD Q values; (iii) together with the DBD-NMEs it also provides the energy spectra of Fermi and Gamow-Teller DCE transition strengths, as well as the locations of the corresponding resonances and their sum rules; (iv) the latter are relevant for both the DBD and the DCE reactions, since the underlying nuclear structure is the same; this correlation does not exist within the *pn*-QRPA model. As an example, detailed numerical calculations are presented for the $(A, Z) \rightarrow (A, Z + 2)$ process in ^{48}Ca $\rightarrow$ ^{48}Ti and the $(A, Z) \rightarrow (A, Z - 2)$ process in ^{96}Ru $\rightarrow$ ^{96}Mo, involving all final 0^+ states and 2^+ states.

DOI: 10.1103/PhysRevC.101.044314

I. INTRODUCTION

The double-charge-exchange (DCE) processes relate the (A, Z) nuclei with the $(A, Z + 2)$ and $(A, Z - 2)$ nuclei and will be labeled as $\{+2\}$ and $\{-2\}$ processes respectively.

The most studied DCE process is the double beta decay (DBD). It is the slowest physical process observed so far, and can be used to learn about neutrino physics, provided we know how to deal with the nuclear structure. According to the number and type of leptons we may have the following DBD modes: (i) double-electron decay ($2\beta^-$), (ii) double-positron decay, (iii) electron capture-positron emitting decay ($e\beta^+$), and (iv) double electron capture decay (ee). Each one of these decays occurs either with the emission of two neutrinos (2ν decay) or they are neutrinoless (0ν decay). To simplify the notation and avoid confusion, we will designate the first process as DBD$^-$ and the remaining three as DBD$^+$.

The 0ν-decay rates depend on several unknown parameters such as neutrino mass, Majoron coupling, the coupling constants of the right-handed components of the weak Hamiltonian, etc., and the only way to put these in evidence is by having sufficient command over the nuclear structure. It is precisely at this point that the $2\nu 2\beta^{\mp}$, $2\nu e\beta^+$, and $2\nu ee$ decay modes are important. A comparison between experiment and theory for them provides a measure of the confidence that one may have in the nuclear wave functions employed for extracting the unknown parameters from 0ν-lifetime measurements.

The number of possible candidates for $2\beta^-$ decay is quite large: there are 35 nuclei. In addition, 34 nuclei can undergo $2e$-electron capture, while 22 and 6 nuclei can undergo $e\beta^+$ and $2\beta^+$ decays respectively [1]. The discovery of the massiveness of the neutrino, through the observation of oscillations, boosted the importance of the 0ν DBD, since they are the only observables capable of providing the magnitude of the effective neutrino mass.

It is well known that the involved nuclear structure in 2ν and 0ν DBD is the same one that describes the DCE reactions. This fact reignited recently the interest in the measurements of heavy-ion-induced DCE reactions, such as the NUMEN project [2–4] involving the ^{40}Ca(^{18}O, ^{18}Ne)^{40}Ar process. Simultaneously, the interest in the theoretical study of the DCE reactions has been renewed [5,6]. Moreover, Shimizu, Menéndez, and Yako [7] have also noted recently a correlation between the DCE and $0\nu 2\beta^-$ decay. In all the theoretical studies mentioned, the calculations were made within the framework of the shell model (SM).

The neutrinoless DBDs occur in medium-mass nuclei that are often far from closed shells and, as a consequence, the calculations are mostly made in the proton-neutron quasiparticle random phase approximation (*pn*-QRPA), since this tool is computationally much simpler than the SM. As discussed in Ref. [8], the kind of correlations that these two methods

*Corresponding author: arsamana@uesc.br

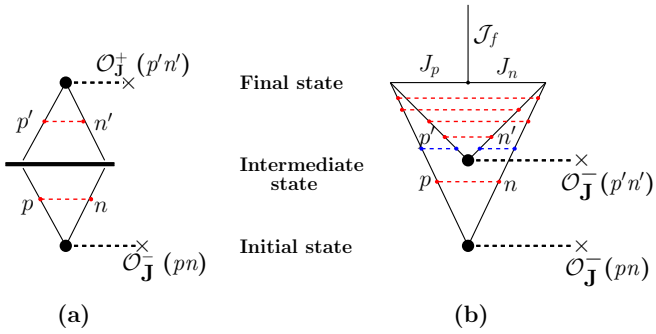

FIG. 1. Graphical representation of the numerators in the $2\beta^-$ NME, where the black points indicate the single β decays. They are (a) $\langle 0^+_f||\mathcal{O}^+_J||J^+_\alpha\rangle\langle J^+_\alpha|J^+_{\alpha'}\rangle\langle J^+_{\alpha'}||\mathcal{O}^-_J|0^+_i\rangle$ in the *pn*-QRPA model, where the overlap between the initial and final QRPA solutions for the intermediate nucleus, $\langle J^+_\alpha|J^+_{\alpha'}\rangle$, is represented by a thick line, and (b) $\langle \mathcal{J}^+_f||\mathcal{O}^-_J||J^+_\alpha\rangle\langle J^+_\alpha||\mathcal{O}^-_J|0^+_i\rangle$ in the $(pn, 2p2n)$-QTDA model, which appears in Eqs. (2.9) and (2.15), and indicates that the first β^- decay is switched on in the initial state and the second in the intermediate state. The $2\beta^+$NMEs are represented in the same way after making the substitution $\mathcal{O}^\mp_J \leftrightarrow \mathcal{O}^\pm_J$. The *pn* and $nn + pp$ nuclear interactions between protons and neutrons are indicated by red and blue dashed lines, respectively. The five vertices of the diagram (b) correspond to five of six angular momentum coupling in the symbol $9j$ in Eq. (2.47). The sixth coupling $(JJ)\mathcal{J}$ corresponds to the three unconnected lines in this figure.

include are not the same. The *pn*-QRPA deals with a large fraction of nucleons in a large single-particle space, but within a modest configuration space. The SM, by contrast, deals with a small fraction of nucleons in a limited single-particle space, but allows them to correlate in arbitrary ways within a large configuration space.

There is another important difference. The standard *pn*-QRPA only allows us to calculate the double-charge-exchange transitions from the ground state of the decaying (A, Z) nucleus to the ground state in the final $(A, Z \pm 2)$ nuclei. In fact, to evaluate the transitions going to the excited states, a second $(pp + nn)$-QRPA must be performed [9,10], which introduces additional free parameters and it is limited to one and two quadrupole phonon states.

To deal with the DCE processes we will resort here to a Tamm-Dancoff approximation (TDA), which has been suggested and discussed on its ph limit (where ph means particle-hole)[1] for ^{48}Ca more than a decade ago in Ref. [11]. In this model it is assumed that the initial, intermediate, and final nuclei are the BCS vacuum, *pn* excitations, and $2p2n$ excitations respectively. The resulting model will be labeled as $(pn, 2p2n)$-QTDA. The main differences with the standard *pn*-QRPA model are illustrated in Fig. 1.

The present model is a natural extension to double-charge-exchange processes of the *pn*-QRPA model, originally proposed by Halbleib and Sorensen (HS) in 1967 to describe single β decays [12]. As such, it permits the evaluation of the NMEs, not only for the ground states but also for all final 0^+ and 2^+ states, as well as the Q values for the $2\beta^-$ decay ($Q_{2\beta^-}$), and for the $2e$ capture (Q_{2e}). It yields as well the DCE energy strength spectra and their sum rules, which are relevant for associated reaction processes and resonances. Detailed numerical calculations are performed in the present work for the ^{48}Ca $\rightarrow$ ^{48}Ti and ^{96}Ru $\rightarrow$ ^{96}Mo processes, involving their final 0^+ and 2^+ states.

II. FORMALISM

A. Nuclear matrix elements and double-charge-exchange excitations

Independently of the nuclear model used, and when only the allowed transitions, i.e., the Gamow-Teller (GT) and Fermi (F) transitions are considered, the NMEs for the $2\nu2\beta^\pm$ decay, from the ground state 0^+_i in the initial nucleus (A, Z) to one of the states 0^+_f in the final nuclei $(A, Z \mp 2)$, reads[2]

$$M^{2\nu^\pm}(0^+_f) = M^{2\nu^\pm}_F(0^+_f) + M^{2\nu^\pm}_{\rm GT}(0^+_f) \equiv \sum_{J=0,1}(-)^J g_J^2 \sum_\alpha \left[\frac{\langle 0^+_f||\mathcal{O}^\pm_J||J^+_\alpha\rangle\langle J^+_\alpha||\mathcal{O}^\pm_J||0^+_i\rangle}{\mathcal{D}^{2\nu^\pm}_{J_\alpha,0_f}}\right], \tag{2.1}$$

where $g_0 \equiv g_V$ and $g_1 \equiv g_A$ are the vector and axial-vector weak coupling constants respectively, and the summation goes over all intermediate virtual states $|J^+_\alpha\rangle$ in the nuclei $(A, Z \mp 1)$.

The one-body operators are

$$\mathcal{O}^-_J = \hat{J}^{-1}\sum_{pn}\langle p||O_J||n\rangle(c^\dagger_p c_{\bar{n}})_J,$$
$$\mathcal{O}^+_J = \hat{J}^{-1}\sum_{pn}\langle n||O_J||p\rangle(c^\dagger_n c_{\bar{p}})_J, \tag{2.2}$$

with $O_0 = 1$, and $O_1 = \sigma$ for F and GT transitions, respectively, $c^\dagger_k \equiv c^\dagger_{j_k,m_k}$ and $c_{\bar{k}} \equiv (-)^{j_k-m_k}c_{j_k,-m_k}$ are the single-particle creation and annihilation operators, and $\hat{J} = \sqrt{2J+1}$.

The energy denominator in Eq. (2.1) is[3]

$$\mathcal{D}^{2\nu^\pm}_{J_\alpha,\mathcal{J}_f} = E^{\{\mp1\}}_{J_\alpha} - \frac{E^{\{0\}}_{0^+} + E^{\{\mp2\}}_{\mathcal{J}_f}}{2} = E^{\{\mp1\}}_{J_\alpha} - E^{\{0\}}_{0^+} + \frac{E^{\{0\}}_{0^+} - E^{\{\mp2\}}_{\mathcal{J}_f}}{2}, \tag{2.3}$$

[1] We consider particle-hole notation, e.g., "ph," as abbreviations and set them in roman font, while we treat "*p*" and "*n*" (denoting proton and neutron, respectively) as particles and set them in italic font.

[2] For the first-forbidden NME see Ref. [13].

[3] The last term in the denominator (2.3) is based on the assumption that the lepton energies can be replaced by $e + \nu \cong (E^{\{0\}}_{0^+} - E^{\{\mp2\}}_{\mathcal{J}_f})/2$, whose validity for the mixed mode was questioned by Hirsch *et al.* [14]. Following their idea on equal sharing of the liberated energy among the emitted leptons, Suhonen [9] has derived formulas for the three different DBD$^+$, and has used them in the evaluation of the decay ^{96}Ru $\rightarrow$ ^{96}Mo. Unfortunately, the author has omitted a factor of 2 in his Eq. (13), which makes the numerical result of mode $2\beta^+$ incorrect. The same error was propagated in subsequent works [15,16]. Here we will continue using the estimate (2.3).

where $E_{0^+}^{\{0\}}$, $E_{J_\alpha}^{\{\pm1\}}$, and $E_{\mathcal{J}_f}^{\{\pm2\}}$ are the energies of the decaying (A, Z) nucleus in its ground state, the intermediate $(A, Z \pm 1)$ nuclei in the state J_α^+, and final $(A, Z \pm 2)$ nuclei in the state $\mathcal{J}_f^+$, respectively.

The matrix elements $\langle J_\alpha^+||\mathcal{O}_J^\pm||0_i^+\rangle$ can be expressed as

$$\langle J_\alpha^+||\mathcal{O}_J^\pm||0_i^+\rangle = \sum_{pn} \rho^\pm\big(pnJ_\alpha^\pi\big) O_J(pn), \tag{2.4}$$

i.e., as a product of model dependent one-body densities,

$$\begin{aligned}\rho^-(pnJ_\alpha) &= \hat{J}^{-1}\langle J_\alpha||(c_p^\dagger c_{\bar{n}})_J||0_i^+\rangle,\\ \rho^+(pnJ_\alpha) &= \hat{J}^{-1}\langle J_\alpha||(c_n^\dagger c_{\bar{p}})_J||0_i^+\rangle,\end{aligned} \tag{2.5}$$

and the single-particle NME,

$$\begin{aligned}O_J(pn) &\equiv \langle p||\mathrm{O}_J||n\rangle\\ &= \delta_{l_p l_n}\sqrt{2}\hat{J}\hat{j}_n\hat{j}_p(-)^{j_p+l_p+J+1/2}\begin{Bmatrix} j_p & j_n & J\\ \frac{1}{2} & \frac{1}{2} & l_n\end{Bmatrix},\end{aligned} \tag{2.6}$$

which is a purely geometric (angular) factor, with the property $O_J(np) = (-)^{j_n-j_p}O_J(pn)$.[4]

Similarly,

$$\langle \mathcal{J}_f^+||\mathcal{O}_J^\pm||J_\alpha^+\rangle = \sum_{np} \rho^\pm(pnJ_\alpha, \mathcal{J}_f^+) O_J(pn), \tag{2.7}$$

where

$$\begin{aligned}\rho^+(pnJ_\alpha, \mathcal{J}_f^+) &= \hat{J}^{-1}\langle \mathcal{J}_f^+||(c_n^\dagger c_{\bar{p}})_J||J_\alpha\rangle,\\ \rho^-(pnJ_\alpha, \mathcal{J}_f^+) &= \hat{J}^{-1}\langle \mathcal{J}_f^+||(c_p^\dagger c_{\bar{n}})_J||J_\alpha\rangle,\end{aligned} \tag{2.8}$$

are the corresponding density matrices for transitions from the intermediate states $|J_\alpha\rangle$ to the final states $|\mathcal{J}_f^+\rangle$, with $\mathcal{J} = 0, 2$.

The corresponding matrix elements are

$$\begin{aligned}M_F^{2\nu^\pm}(0_f^+) &= g_V^2 \sum_\alpha \frac{\langle 0_f^+||\mathcal{O}_0^\pm||0_\alpha^+\rangle\langle 0_\alpha^+||\mathcal{O}_0^\pm|0_i^+\rangle}{\mathcal{D}^{2\nu^\pm}_{0_\alpha^+,0_f^+}},\\ M_{\mathrm{GT}}^{2\nu^\pm}(\mathcal{J}_f^+) &= \frac{-g_A^2}{\sqrt{\mathcal{J}+1}} \sum_\alpha \frac{\langle \mathcal{J}_f^+||\mathcal{O}_1^\pm||1_\alpha^+\rangle\langle 1_\alpha^+||\mathcal{O}_1^\pm|0_i^+\rangle}{\big(\mathcal{D}^{2\nu^\pm}_{1_\alpha^+,\mathcal{J}_f^+}\big)^{\mathcal{J}+1}},\end{aligned} \tag{2.9}$$

where the GT-NMEs to 2_f^+ states have also been included [17–19].

All the information about the nuclear structure is contained in the one-body density matrices (2.4) and (2.8) or, more precisely, in the two-body density matrices,

$$\rho^\pm(pnp'n'; J_\alpha, \mathcal{J}_f^+) = \rho^\pm(pn; J_\alpha)\rho^\pm(p'n'; J_\alpha, \mathcal{J}_f^+). \tag{2.10}$$

The NME for the $0\nu2\beta^\pm$ decays to the 0_f^+ final states can be easily evaluated from these densities. In fact, after making the replacement in Ref. [[20], Eqs. (2.20)]

$$\rho^{\mathrm{ph}}(pnp'n'; J_\alpha) \to \rho^\pm(pnp'n'; J_\alpha, \mathcal{J}_f^+), \tag{2.11}$$

we can express them as

$$M^{0\nu^\pm}(0_f^+) = \sum_X M_X^{0\nu^\pm}(0_f^+), \tag{2.12}$$

where $X = V, A, P, M$ stands for vector (V), axial-vector (A), pseudoscalar (P), and weak-magnetism (M) terms. With the NME $M^{0\nu^\pm}(2_f^+)$ we proceed in the same way.

It is well known that the single β-decay processes to the states J_α in $(A, Z+1)$ and $(A, Z-1)$ nuclei are related to the following single charge-exchange transition strengths:

$$S_J^{\{\pm1\}} \equiv \sum_\alpha B_{J_\alpha}^{\{\pm1\}} = \hat{J}^{-2}\sum_\alpha |\langle J_\alpha^+||\mathcal{O}_J^\mp||0_i^+\rangle|^2. \tag{2.13}$$

When $|J_\alpha^+\rangle$ is a complete set of excited states that can be reached by operating with $\mathcal{O}_J^\pm$ on the initial state $|0_i^+\rangle$, they satisfy the single-charge exchange (SCE) or Ikeda sum rule, for both the F and GT transitions,

$$S_J^{\{1\}} \equiv S_J^{\{+1\}} - S_J^{\{-1\}} = (-)^J\hat{J}^{-2}\langle 0_i^+|[\mathcal{O}_J^-, \mathcal{O}_J^+]_0|0_i^+\rangle = N - Z. \tag{2.14}$$

Similarly, both $M^{2\nu2\beta^\pm}(\mathcal{J}_f^+)$ and $M^{0\nu2\beta^\pm}(\mathcal{J}_f^+)$ are related to the double-charge-exchange operators $(\mathcal{O}_J^\pm\mathcal{O}_J^\pm)_\mathcal{J}$ and to their spectral distributions in $(A, Z \pm 2)$ nuclei given by

$$S_{J\mathcal{J}}^{\{\pm2\}} \equiv \sum_f B_{J\mathcal{J}_f}^{\{\pm2\}} = \hat{J}^{-2}\sum_f \left|\sum_\alpha \langle \mathcal{J}_f^+||\mathcal{O}_J^\mp||J_\alpha^+\rangle\langle J_\alpha^+||\mathcal{O}_J^\mp|0_i^+\rangle\right|^2. \tag{2.15}$$

When both $|J_\alpha^+\rangle$ and $|\mathcal{J}_f^+\rangle$ are a complete set of excited states that can be reached by operating with $\mathcal{O}_J^\pm$, and $(\mathcal{O}_J^\pm\mathcal{O}_J^\pm)_\mathcal{J}$ on the initial state $|0_i^+\rangle$, their differences

$$\begin{aligned}S_{J\mathcal{J}}^{\{2\}} &= S_{J\mathcal{J}}^{\{+2\}} - S_{J\mathcal{J}}^{\{-2\}}\\ &= \hat{J}^{-2}\sum_f \left[\left|\sum_\alpha \langle \mathcal{J}_f^+||\mathcal{O}_J^-||J_\alpha^+\rangle\langle J_\alpha^+||\mathcal{O}_J^-|0_i^+\rangle\right|^2\right.\\ &\quad \left. - \left|\sum_\alpha \langle \mathcal{J}_f^+||\mathcal{O}_J^+||J_\alpha^+\rangle\langle J_\alpha^+||\mathcal{O}_J^+|0_i^+\rangle\right|^2\right]\end{aligned} \tag{2.16}$$

obey the double-charge-exchange sum rules (DCESRs), which were evaluated in Refs. [5,6,21–23] with the following results:

$$\mathsf{S}_{\mathrm{DF}} \equiv \mathsf{S}_{00}^{\{2\}} = 2(N-Z)(N-Z-1), \tag{2.17}$$

$$\begin{aligned}\mathsf{S}_{\mathrm{DGT},0} &\equiv \mathsf{S}_{10}^{\{2\}}\\ &= 2(N-Z)\big(N-Z+1+2S_1^{\{-1\}}\big) - \tfrac{2}{3}C,\end{aligned} \tag{2.18}$$

$$\begin{aligned}\mathsf{S}_{\mathrm{DGT},2} &\equiv \mathsf{S}_{12}^{\{2\}}\\ &= 10(N-Z)\big(N-Z-2+2S_1^{\{-1\}}\big) + \tfrac{5}{3}C,\end{aligned} \tag{2.19}$$

where C is a relatively small quantity given by [[22], Eq. (4)]. These equations agree with Eq. (8) in Ref. [6] except for a factor of 3 and the omission of $S_1^{\{-1\}}$.

[4] We use here the angular momentum coupling scheme $|(\frac{1}{2}, l)j\rangle$.

Combining Eqs. (2.18) and (2.19), one obtains the sum rule for the total GT strength,

$$\mathrm{S_{DGT}} = 12(N-Z)\big(N-Z-\tfrac{3}{2}+2S_1^{\{-1\}}\big)+C, \quad (2.20)$$

which is independent of the structure of the ground-state wave function [22].

The relationship between the DBD and DCE reactions has been discussed recently in Refs. [2,7].

B. (*pn*, 2*p*2*n*)-QTDA model

The *pn*-QRPA evaluations of the DBDs are generally limited to the ground state of the final nuclei, i.e., to the calculation of $M_{2\nu}(0_1^+)$ and $M_{0\nu}(0_1^+)$. Moreover, the SCESRs (2.14) are fulfilled within this model, but it does not allow us to evaluate the strengths $S_{J\mathcal{J}}^{2\beta^\pm}$ given by (2.16) and to discuss the corresponding DCESRs listed in Eqs. (2.17)–(2.20).

To describe the intermediate states J_α^+ in both *pn*-QRPA and (*pn*, 2*p*2*n*)-QTDA models a nuclear Hamiltonian of the type

$$H_1 = H_0 + H_{pn} \quad (2.21)$$

is used, where

$$H_0 = \sum_\alpha E_k a_k^\dagger a_k \quad (2.22)$$

is the independent-quasiparticle Hamiltonian, with $a_\alpha^\dagger$ and $a_{\bar\alpha}$ being the single-quasiparticle creation and annihilation operators, defined by the Bogoliubov transformation [[24], Eqs. (13.10)]

$$\begin{aligned} a_k^\dagger &= u_a c_k^\dagger + v_k c_{\bar k}, \\ a_{\bar k} &= u_a c_{\bar k} - v_a c_k^\dagger. \end{aligned} \quad (2.23)$$

The proton and neutron pairing interactions are contained in the transformation coefficients u_a and v_a, and in the quasiparticle energy

$$E_k = \big[(e_k-\lambda)^2+\Delta_k^2\big]^{1/2}, \quad (2.24)$$

where e_k is the shell-model single-particle energy (spe), and λ is the chemical potential or Fermi level. The energy gap parameters Δ_k and the pairing coupling constants are determined to reproduce the experimental odd-mass difference for each nucleus. Finally, H_{pn} is the quasiproton-quasineutron interaction.

Within the *pn*-QRPA, the states $|J_\alpha\rangle$ with excitation energy ω_{J_α} are created from the correlated initial and final 0^+ ground states by proton-neutron phonon creation operators Q_{J_α}, which are defined as a linear superposition of creation and annihilation proton-neutron quasiparticle pair operators

$$\begin{aligned} A^\dagger(pnJ) &\equiv A^\dagger(pnJM) = [a_p^\dagger a_n^\dagger]_{JM}, \\ A(pn\bar J) &= (-)^{J-M} A(pnJ,-M). \end{aligned} \quad (2.25)$$

That is,

$$|J_\alpha\rangle = Q_{J_\alpha}^\dagger|0^+\rangle \equiv \sum_{pn}\big[X_{pnJ}^\alpha A^\dagger(pnJ) - Y_{pnJ}^\alpha A(pn\bar J)\big]|0^+\rangle, \quad (2.26)$$

and

$$Q_{J_\alpha}|0^+\rangle = 0, \quad H_1|J_\alpha\rangle = \omega_{J_\alpha}|J_\alpha\rangle. \quad (2.27)$$

Frequently, this is done for both initial $|0_I^+\rangle$ and final $|0_F^+\rangle$ ground states, obtaining in this way two different sets of intermediate states J_α and $J_{\alpha'}$ in the $(N-1, Z+1)$ nucleus. Therefore, in the evaluation of the 2β-NME, it is necessary to consider their overlap, which is indicated in Fig. 1, and corresponds to the substitution

$$\begin{aligned} \sum_{J_\alpha}\rho^{\mathrm{ph}}(pnp'n';J_\alpha) &\to \langle 0_I^+|0_F^+\rangle \\ &\times \sum_{J^\pi\alpha\alpha'}\rho^+(p'n';J_{\alpha'})\langle J_{\alpha'}|J_\alpha\rangle\rho^-(pn;J_\alpha). \end{aligned} \quad (2.28)$$

The ground state defined in Eq. (2.27) is more accurate than the BCS ground state ($a_k|\mathrm{BCS}\rangle = 0$) since it contains terms with $0, 4, 8, \ldots$ quasiparticles [8]. Nevertheless, in the present model we approximate the initial ground state in the (A, Z) nucleus by the BCS vacuum and the states $|J_\alpha\rangle$ in the intermediate $(A, Z\mp1)$ nuclei as

$$\begin{aligned} |J_\alpha\rangle &= \sum_{pn} X_{pnJ_\alpha} A^\dagger(pnJ)|\mathrm{BCS}\rangle, \\ H_1|J_\alpha\rangle &= \omega_{J_\alpha}|J_\alpha\rangle. \end{aligned} \quad (2.29)$$

This disadvantage of the present model is counteracted by the description that we make of the final states in the $(A, Z\mp2)$ nuclei; that is, instead of the correlated $|0_F^+\rangle$ state defined in Eq. (2.26), we have

$$|\mathcal{J}_f^+\rangle = \sum_{p_1p_2n_1n_2J_pJ_n} \mathcal{X}_{p_1p_2J_p,n_1n_2J_n;\mathcal{J}_f^+}|p_1p_2J_p, n_1n_2J_n;\mathcal{J}^+\rangle_A, \quad (2.30)$$

where $\mathcal{J}^+ = 0^+, 2^+$ and

$$|p_1p_2J_p, n_1n_2J_n;\mathcal{J}^+\rangle_A = [\mathcal{A}^\dagger(p_1p_2J_p)\mathcal{A}^\dagger(n_1n_2J_n)]^{\mathcal{J}^+}|\mathrm{BCS}\rangle, \quad (2.31)$$

are antisymmetrized and normalized two-proton-two-neutron quasiparticle states, where

$$\mathcal{A}^\dagger(abJ) = N(ab)A^\dagger(abJ), \quad N(ab) = \frac{1}{\sqrt{1+\delta_{ab}}} \quad (2.32)$$

are normalized two-quasiparticle states.

The amplitudes $\mathcal{X}_{p_1p_2J_{12},n_1n_2J'_{12};\mathcal{J}_f^+}$ are obtained by diagonalizing the Hamiltonian [25,26]

$$\begin{aligned} H_2 &= H_0 + H_{pn} + H_{nn} + H_{pp}, \\ H_2|\mathcal{J}_f^+\rangle &= \omega_{\mathcal{J}_f^+}|\mathcal{J}_f^+\rangle, \end{aligned} \quad (2.33)$$

in the basis (2.31) where H_{nn} and H_{pp} are neutron-neutron and proton-proton interactions. Details on the evaluation of matrix elements of H_2 can be found in Refs. [25,26]. However, our final results are different.

The matrix element of H_{pn} for the odd-odd nucleus reads

$$\begin{aligned} &\langle\mathrm{BCS}|A(npJ)H_{pn}A^\dagger(n'p'J)|\mathrm{BCS}\rangle \\ &= G(npn'p'J)(u_pu_nu_{p'}u_{n'} + v_pv_nv_{p'}v_{n'}) \\ &\quad + F(npn'p'J)(u_pv_nu_{p'}v_{n'} + v_pu_nv_{p'}u_{n'}), \end{aligned} \quad (2.34)$$

where the functions G and F are defined in the standard way [25,26]. They differ from those of Baranger [27] by a factor of -2, as can be seen, for example, from the comparison of [[27], Eq. (20)] with [[28], Eq. (4)] (or with [[29], Eq. (3.2)]). Our G and F functions are also different from those of Suhonen [24].

The matrix elements of H_{pn} in the basis (2.31) are derived by employing the relation (1A-25) from [30]. We get

$$\begin{aligned}
&\langle \mathrm{BCS}|[\mathcal{A}^\dagger(n_1n_2J_n)\mathcal{A}^\dagger(p_1p_2J_p)]^{\mathcal{J}\dagger}H_{pn}[\mathcal{A}^\dagger(n_1'n_2'J_n')\mathcal{A}^\dagger(p_1'p_2'J_p')]^{\mathcal{J}}|\mathrm{BCS}\rangle \\
&= \hat{J}_n\hat{J}_p\hat{J}_n'\hat{J}_p' N(n_1n_2)N(n_1'n_2')N(p_1p_2)N(p_1'p_2')\bar{P}(n_1n_2J_n)\bar{P}(p_1p_2J_p) \\
&\times \bar{P}(n_1'n_2'J_n')\bar{P}(p_1'p_2'J_p')\sum_{J_1J_2}\hat{J}_1^2\hat{J}_2^2\begin{Bmatrix} n_1 & n_2 & J_n \\ p_1 & p_2 & J_p \\ J_1 & J_2 & \mathcal{J}\end{Bmatrix}\begin{Bmatrix} n_1' & n_2' & J_n' \\ p_1' & p_2' & J_p' \\ J_1 & J_2 & \mathcal{J}\end{Bmatrix} \\
&\times \langle \mathrm{BCS}|A(n_1p_1J_1)H_{pn}A^\dagger(n_1'p_1'J_1)|\mathrm{BCS}\rangle\delta_{p_2p_2'}\delta_{n_2n_2'},
\end{aligned} \tag{2.35}$$

where the operator

$$\bar{P}(p_1p_2J) = 1 + (-)^{p_1-p_2+J}P(p_1 \leftrightarrow p_2), \tag{2.36}$$

exchanges the particles p_1 and p_2.

Finally, the matrix element of the neutron-neutron Hamiltonian H_{nn} in the same basis is

$$\begin{aligned}
&\langle \mathrm{BCS}|[\mathcal{A}^\dagger(n_1n_2J_n)\mathcal{A}^\dagger(p_1p_2J_p)]^{\mathcal{J}\dagger}H_{nn}[\mathcal{A}^\dagger(n_1'n_2'J_n')\mathcal{A}^\dagger(p_1'p_2'J_p')]^{\mathcal{J}}|\mathrm{BCS}\rangle \\
&= \delta_{J_pJ_p'}\delta_{J_nJ_n'}\delta_{p_1p_1'}\delta_{p_2p_2'}\langle \mathrm{BCS}|\mathcal{A}(n_1n_2J_n)H_{nn}\mathcal{A}^\dagger(n_1'n_2'J_n)|\mathrm{BCS}\rangle \\
&= \delta_{J_pJ_p'}\delta_{J_nJ_n'}\delta_{p_1p_1'}\delta_{p_2p_2'}N(n_1n_2)N(n_1'n_2')\big[\big(u_{n_1}u_{n_2}u_{n_1'}u_{n_2'} + v_{n_1}v_{n_2}v_{n_1'}v_{n_2'}\big)G(n_1n_2n_1'n_2'J_n) \\
&+ \big(u_{n_1}v_{n_2}u_{n_1'}v_{n_2'} + v_{n_1}u_{n_2}v_{n_1'}u_{n_2'}\big)F(n_1n_2n_1'n_2'J_n) - (-1)^{n_1+n_2-J_n}\big(u_{n_1}v_{n_2}v_{n_1'}u_{n_2'} + v_{n_1}u_{n_2}u_{n_1'}v_{n_2'}\big)F(n_2n_1n_1'n_2'J_n)\big],
\end{aligned} \tag{2.37}$$

and analogously for the proton-proton Hamiltonian H_{pp}.

The energies in the denominator $\mathcal{D}^{2\nu^\pm}_{J_\alpha,\mathcal{J}_f}$, defined by (2.3), are

$$\begin{aligned}
E^{\{\pm1\}}_{J_\alpha} - E^{\{0\}}_{0^+} &= \omega_{J_\alpha} \pm \lambda_p \mp \lambda_n, \\
E^{\{\pm2\}}_{\mathcal{J}_f} - E^{\{0\}}_{0^+} &= \omega_{\mathcal{J}_f} \pm 2\lambda_p \mp 2\lambda_n,
\end{aligned} \tag{2.38}$$

where λ_p and λ_n are the proton and neutron chemical potentials. Therefore, for both $2\beta^+$ and $2\beta^-$ decays we have

$$\mathcal{D}^{2\nu^\pm}_{J_\alpha,\mathcal{J}_f} \equiv \mathcal{D}^{2\nu}_{J_\alpha,\mathcal{J}_f} = \omega_{J_\alpha} - \frac{\omega_{\mathcal{J}_f}}{2}. \tag{2.39}$$

The lowest energies $E^{\{\pm2\}}_{0_f^+}$ are directly related with the Q values for the $2\beta^-$ decay ($Q_{2\beta^-}$) and for the $2e$ capture (Q_{2e}), defined as[5]

$$\begin{aligned}
Q_{2\beta^-} &= \mathcal{M}(Z,A) - \mathcal{M}(Z+2,A), \\
Q_{2e} &= \mathcal{M}(Z,A) - \mathcal{M}(Z-2,A),
\end{aligned} \tag{2.40}$$

where the $\mathcal{M}$'s are the atomic masses. Namely,

$$\begin{aligned}
Q_{2\beta^-} &= E^{\{0\}}_{0^+} - E^{\{+2\}}_{0_1^+} = -\omega_{0_1^+} - 2(\lambda_p - \lambda_n), \\
Q_{2e} &= E^{\{0\}}_{0^+} - E^{\{-2\}}_{0_1^+} = -\omega_{0_1^+} + 2(\lambda_p - \lambda_n).
\end{aligned} \tag{2.41}$$

[5]The $2\beta^+$ and β^+e Q values are

$$\begin{aligned}
Q_{2\beta^+} &= \mathcal{M}(Z,A) - \mathcal{M}(Z-2,A) - 4m_e, \\
Q_{\beta^+e} &= \mathcal{M}(Z,A) - \mathcal{M}(Z-2,A) - 2m_e.
\end{aligned}$$

Note that $Q_{2e} - Q_{2\beta^-} = 4(\lambda_p - \lambda_n)$ and $Q_{2e} + Q_{2\beta^-} = -2\omega_{0_1^+}$.

To evaluate the one-body densities (2.4) and (2.8) we make use of [[24], Eqs. (15.4)] to get

$$\begin{aligned}
(c_p^\dagger c_{\bar{n}})_J &\to u_pv_nA^\dagger(pnJ), \\
(c_n^\dagger c_{\bar{p}})_J &\to u_nv_pA^\dagger(npJ),
\end{aligned} \tag{2.42}$$

which, from (2.2) and (2.5), immediately yields

$$\rho^\pm(pnJ_\alpha) = X_{pnJ_\alpha}\begin{Bmatrix} u_nv_p \\ u_pv_n\end{Bmatrix} \tag{2.43}$$

and

$$\langle J_\alpha^+||\mathcal{O}_J^\pm||0_i^+\rangle = \sum_{pn} X_{pnJ_\alpha}O_J^\pm(pn), \tag{2.44}$$

with

$$O_J^\pm(pn) = O_J(pn)\begin{Bmatrix} u_nv_p \\ u_pv_n\end{Bmatrix}. \tag{2.45}$$

The derivation of $\langle \mathcal{J}_f^+||\mathcal{O}_J^\pm||J_\alpha^+\rangle$ is more involved and one gets

$$\begin{aligned}
&\langle \mathcal{J}_f^+||\mathcal{O}_J^\pm||J_\alpha^+\rangle \\
&= \hat{J}\hat{\mathcal{J}}_f\sum_{pnp'n'J_pJ_n}(-)^{J_p+J_n}\hat{J}_p\hat{J}_n \\
&\times N(nn')N(pp')\mathcal{X}_{pp'J_p,nn'J_n;\mathcal{J}_f^+}\bar{P}(nn'J_n)\bar{P}(pp'J_p) \\
&\times \begin{Bmatrix} p & p' & J_p \\ n & n' & J_n \\ J & J & \mathcal{J}\end{Bmatrix}X_{p'n'J_\alpha}O_J^\pm(pn).
\end{aligned} \tag{2.46}$$

The densities $\rho^{\pm}(pn; J^{\pi}_{\alpha}, \mathcal{J}^{+}_{f})$ result immediately (2.7) and (2.46).

Making use of orthogonality and completeness of both basis $|J_{\alpha}\rangle$ and $A^{\dagger}(pnJ)|\mathrm{BCS}\rangle$ in Eq. (2.29), the relation (2.15) can be expressed in a more compact form, namely as

$$B^{\{\pm 2\}}_{J\mathcal{J}} = \hat{\mathcal{J}}^2 \Bigg| \sum_{pp'nn'J_pJ_n} (-)^{J_p+J_n} \hat{J}_p \hat{J}_n N(nn') N(pp') \times \mathcal{X}_{pp'J_p,nn'J_n;\mathcal{J}^{+}_{f}} \bar{P}(nn'J_n) \bar{P}(pp'J_p) \times \begin{Bmatrix} p & p' & J_p \\ n & n' & J_n \\ J & J & \mathcal{J} \end{Bmatrix} O^{\mp}_{J}(p'n') O^{\mp}_{J}(pn) \Bigg|^2 . \quad (2.47)$$

In this way, the transition strength turns out to be independent of the intermediate states.

It is important to emphasize that the permutation operators in the last two equations only act on the right side. The physical meaning of these permutations can be inferred from Fig. 1(b), where the DCE matrix element $\sum_{\alpha} \langle \mathcal{J}^{+}_{f} || \mathcal{O}^{-}_{J} || J^{+}_{\alpha} \rangle \langle J^{+}_{\alpha} || \mathcal{O}^{-}_{J} | 0^{+}_{i} \rangle$ is represented graphically. This quantity is used in the evaluation of both the DBD NME (2.9) and the DCE transition strengths (2.15), but the Eq. (2.47) is applicable only in the latter case.

Together with the NMEs $M^{2\nu^{\pm}}(\mathcal{J}^{+}_{f})$ given by (2.1) and (2.9) with $M^{2\nu^{\pm}}(2^{+}_{f}) \equiv M^{2\nu^{\pm}}_{\mathrm{GT}}(2^{+}_{f})$, we will also evaluate the half-lives $\tau^{\alpha}_{2\nu}(\mathcal{J}^{+}_{f})$ for different $\alpha(=2\beta^{-}, 2\beta^{+}, e\beta^{+}, 2e)$. This is done from

$$\left[\tau^{\alpha}_{2\nu}(\mathcal{J}^{+}_{f})\right]^{-1} = g^{4}_{A} |M^{2\nu^{\pm}}(\mathcal{J}^{+}_{f})|^2 G^{\alpha}_{2\nu}(\mathcal{J}^{+}_{f}), \quad (2.48)$$

where the NMEs are given in natural units ($\hbar = m_e = c = 1$), and the leptonic kinematics factors, $G^{\alpha}_{2\nu}(\mathcal{J}^{+}_{f})$, are in yr^{-1}. These factors can be found in Ref. [[31], Table II] for several nuclei of interest. (For the most recent computations of phase space factors see Refs. [32,33].)

The excitation energies in the final nuclei are calculated from

$$\mathcal{E}_{f} = E^{\{+2\}}_{0^{+}_{f}} - E^{\{+2\}}_{0^{+}_{1}}. \quad (2.49)$$

It should be noted that, just as the *pn*-QRPA model predicts identical excitation energies for the $(Z, A \pm 1)$ nuclei, the current model yields the same the excitation energies in the $(Z, A \pm 2)$ nuclei.

Finally, the centroid energies of the DCE transition strengths are defined as

$$\bar{E}^{\{\pm 2\}}_{J\mathcal{J}} = \frac{\sum_{f} \mathcal{E}_{\mathcal{J}^{+}_{f}} B^{\{\pm 2\}}_{J\mathcal{J}_{f}}}{S^{\{\pm 2\}}_{J\mathcal{J}}}. \quad (2.50)$$

III. NUMERICAL RESULTS AND DISCUSSION

The residual interaction is described by the δ force (in units of MeV fm^3)

$$V = -4\pi (v_s P_s + v_t P_t) \delta(r), \quad (3.1)$$

where v_s and v_t are the spin-singlet and spin-triplet parameters.

TABLE I. Results for the BCS coupling constants and Fermi levels. All notation is explained in the text. The λ's are given in units of MeV, and the couplings v^{pair}_{s} is in units of MeV fm^3.

Nuclei	spe	$v^{\mathrm{pair}}_{s}(n)$	$v^{\mathrm{pair}}_{s}(p)$	λ_n	λ_p
^{48}Ca	e^{expt}_{j}	31.45	34.77	−6.587	−13.000
	e_j	25.20	28.35	−7.091	−12.702
^{96}Ru		33.20	38.91	−8.412	−5.663

A. Mean field

The mean field is defined by the unperturbed Hamiltonian H_0 and the spe that are specified below. As usual, the pairing strengths for protons and neutrons, $v^{\mathrm{pair}}_{s}(p)$ and $v^{\mathrm{pair}}_{s}(n)$, are obtained from the fitting of the experimental pairing gaps.

The DBD$^-$ $^{48}\mathrm{Ca} \rightarrow {}^{48}\mathrm{Ti}$ is a rather unique case, since ^{48}Ca is a double closed nuclei, and we can make use of the experimental spe, labeled as e^{expt}_{j}, which comprises the energies of both the single-particle and single-hole states. All of them were taken from the binding and excitation energies, weighted with spectroscopic factors, of odd-mass neighboring nuclei: ^{47}Ca and ^{49}Ca for neutrons, and ^{47}K and ^{49}Sc for protons. They are listed in Fig. 2 and are those from [[34], Table II], except for the proton $f_{5/2}$ spe, which is estimated from the proton $f_{5/2}$-$f_{7/2}$ splitting given in Ref. [35]. We need this level to saturate both the SCE and DCE sum rules. Once this has been done, the spe e^{expt}_{j} have been used in two different ways:

(1) The following steps are done in handling the BCS equations [13,36,37]:
   (a) The BCS energies relative to the Fermi level λ,
   $$E^{(\pm)}_{j} = \pm E_j + \lambda, \quad (3.2)$$
   are introduced, where the positive (negative) sign is adopted if the corresponding single-particle state is a particle (hole) state.
   (b) It is assumed that neutron and proton Fermi levels λ_n and λ_p lay between $j_n = 2p_{3/2}$-$1f_{7/2}$ and $j_p = 1f_{7/2}$-$1d_{3/2}$ states respectively, and that all states above λ are pure quasiparticle excitations $E^{(+)}_{j}$ and all states below λ are pure quasihole excitations $E^{(-)}_{j}$.
   (c) Starting from a set of harmonic oscillator energies e^{HO}_{j}, the energies $E^{(\pm)}_{j}$ are adjusted to the experimental spectra e^{expt}_{j} by means of a χ^2 search varying the strengths v^{pair}_{s} and the bare spe e_j which that appear in the BCS gap equations (2.24). All energies involved in this procedure are illustrated in Fig. 2.
(2) For the sake of completeness, the pairing parameters $v^{\mathrm{pair}}_{s}(p)$ and $v^{\mathrm{pair}}_{s}(n)$ were fixed in the standard manner [29]. That is, by fitting the experimental pairing gaps to the calculated pairing gaps Δ_j, given by [[30], Eq. (2.96)], with $j = 1f_{7/2}$ for neutrons and $j = 2s_{1/2}$ for protons.

The most relevant difference between the spe e^{expt}_{j} and e_j is the disappearance of the energy gap between the holes and the particles in the last case. The resulting parameters v^{pair}_{s},

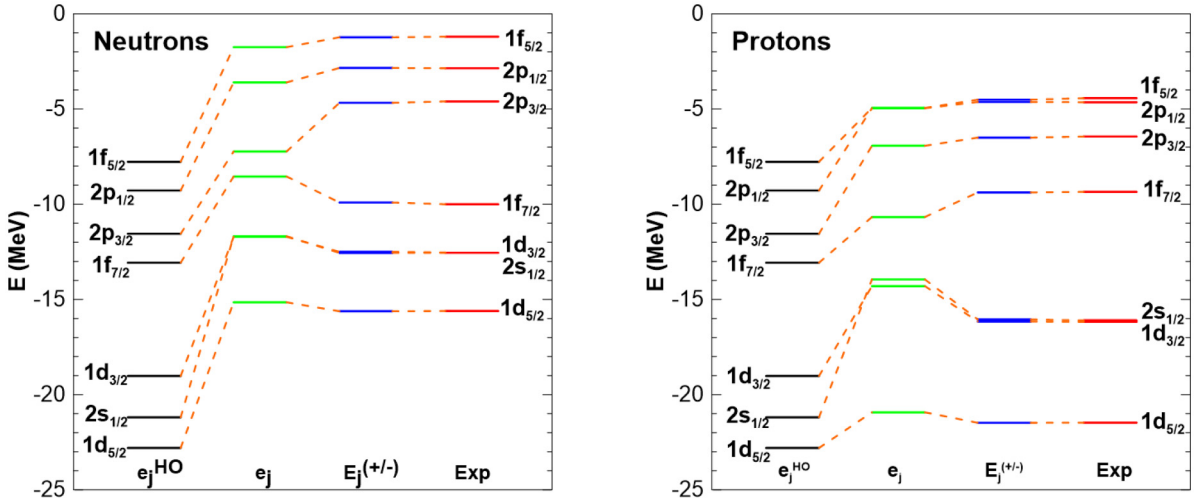

FIG. 2. Mean field energies (in units of MeV) for neutrons (left panel) and for protons (right panel). In both cases we show (i) harmonic oscillator energies $e_j^{\rm HO}$, (ii) adjusted single-particle energies e_j, (iii) BCS energies relative to the Fermi level ($E_j^{(\pm)}$), and (iv) experimental energies ($e_j^{\rm expt}$).

and λ are given in the Table I for the two sets of spe e_j and $e_j^{\rm expt}$. The quasiparticle energies $E_j^{(\pm)}$ with $e_j^{\rm expt}$ are obviously slightly different from those shown in Fig. 2.

In the ^{96}Ru nucleus, the neutron and proton shells are open and its energy spectrum is clearly rotational. This fact gives rise to a strong interplay between collective and single-particle degrees of freedom in the low energy spectra of the neighboring odd-mass nuclei ^{95}Ru, ^{97}Ru, ^{95}Tc, and ^{97}Rh. For instance, it is very likely that the ground state $5/2^+$ in ^{95}Ru is a consequence of the $j-1$ anomaly in the three neutron cluster $(1g_{7/2})^3$ [38,39]. Such a complex nuclear structure makes it to difficult determine the appropriate spe spectra and the pairing interaction strengths from experimental energy spectra, as it was done in the case of ^{48}Ca.

Instead, we used the spe provided by Paar [40], which were calculated in the relativistic Hartree-Bogoliubov model, as outlined in Ref. [41]. They are shown in Table II, together with the resulting quasiparticle energies (3.3), which were obtained following procedure 2 in the case of ^{48}Ca. This suggests fitting the calculated pairing gaps Δ_j, with $j = 1g_{7/2}$ for neutrons and $j = 1g_{9/2}$ for protons, to the experimental ones. The similarity between the spe e_j and the quasiparticle energies $E_j^{(\pm)}$ is remarkable. The corresponding pairing parameters $v_s^{\rm pair}$ and chemical potentials λ are listed in Table I.

TABLE II. Neutron and proton spe for ^{96}Ru, which were obtained in the manner explained in the text, together with the resulting quasiparticle energies (3.3). All notation is explained in the text. The energies are given in units of MeV.

	Neutrons		Protons	
Level	e_j	$E_j^{(\pm)}$	e_j	$E_j^{(\pm)}$
$3s_{1/2}$	−5.396	−5.182	4.916	5.006
$2d_{3/2}$	−5.236	−4.983	4.792	4.897
$1g_{7/2}$	−6.878	−6.527	2.308	2.502
$2d_{5/2}$	−7.401	−10.051	2.493	2.627
$1g_{9/2}$	−14.401	−14.500	−5.424	−7.448
$2p_{1/2}$	−17.802	−17.913	−7.718	−8.478
$2p_{3/2}$	−19.389	−19.484	−9.295	−9.773

It is important to note that in ^{48}Ca it is $\lambda_n > \lambda_p$ while in ^{76}Ru this difference is $\lambda_n < \lambda_p$. We will soon see that this fact is decisive with respect to the Q values of DBD. More precisely, this will explain why DBD$^-$ occurs in ^{48}Ca and DBD$^+$ occurs in ^{96}Ru.

Our method of calculation is similar in several aspects to that used in the SM framework in Refs. [5,6]. In fact, the illustration of their calculations, made in Fig. 1 of the last reference, is also valid in our case. The biggest difference between the two models, in addition to the residual interactions that were used, arises from the size of the configuration spaces of the final states $\mathcal{J}_f^+$. We have 664 0^+ states and 2.470 2^+ states, while Auerbach and Bui Minh Loc [6] have, in their evaluation of double-charge-exchange GT strength ^{48}Ca $\rightarrow$ ^{48}Ti, the quantity of 14.177 and 61.953 final states in the fp space, respectively. In the case of the ^{96}Ru $\rightarrow$ ^{96}Mo decay, we also have 664 0^+ states, but 2.583 2^+ states.[6]

B. Residual interaction

The same coupling constants $v_s^{\rm pp}$, $v_t^{\rm pp}$, $v_s^{\rm ph}$, and $v_t^{\rm ph}$ were used in the numerical evaluations of the matrix elements of the Hamiltonians H_{pn}, H_{pp}, H_{nn}, given by Eqs. (2.34) and (2.37).

That is, we assume that the residual interaction is the same for identical and nonidentical particles, which is a very strong constraint on the model parameters.

[6]See also our Fig. 1, where the difference between our model with the standard pn-QRPA calculation of the NME is illustrated graphically.

In all our previous works within the *pn*-QRPA model [20,28,42–47] the values of the interaction coupling constants, both in ph and pp channels, were set from the partial restoration of the spin-isospin SU(4) symmetry (PSU4SR) induced by the residual interaction. The corresponding physical motivations for this, and the procedure are discussed in those references in detail. However, to make the present paper self-contained, it might be appropriate to use some paragraphs to explain the philosophy of the PSU4SR approach. In doing this, we necessarily have to partially repeat what has been said previously, in particular in Ref. [47].

(1) *Particle-hole channel*. The SU(4) symmetry is dynamically broken by the spin-orbit coupling and the supermultiplet destroying residual interactions, but these two effects have a tendency to cancel each other. Indeed, it is an experimental fact that the energy difference between the GT resonance and the isobaric analog state (IAS) behaves as

$$E_{\rm GT} - E_{\rm IAS} = 26A^{-1/3} - 18.5(N-Z)/A, \qquad (3.3)$$

where the first and second terms are interpreted as arising from the mean spin-orbit splitting and the difference in the corresponding residual interactions, when described within the TDA [48–50], respectively. Moreover, for the residual interaction (3.1), the last term in Eq. (3.3) implies that

$$v_t^{\rm ph} - v_s^{\rm ph} = 37\ {\rm MeV\,fm}^3, \qquad (3.4)$$

and we say that the PSU4SR takes place within the ph channel when this condition is met.

(2) *Particle-particle channel*. For a system with $N \neq Z$, the isospin and spin-isospin symmetries are violated in the mean field approximation, since the neutron excess automatically yields isovector mean fields, i.e., different Hartree-Fock (HF) potentials for protons and neutrons. This occurs even if the nuclear Hamiltonian commutes with the corresponding excitation operators $\mathcal{O}_J^{\pm}$.

However, it was very early realized that when a nondynamical violation occurs in the HF solution, the RPA-induced ground state correlations (GSCs) can be invoked to restore the symmetry [51–54]. These correlations are not explicitly evidenced, but only implicitly through their effects on the matrix elements and the corresponding decay rates [see, for instance, Eqs. (3.7) and (3.8) below].

Here it is convenient to define the ratios

$$s = \frac{v_s^{\rm pp}}{\overline{v}_s^{\rm pair}}, \quad \text{and} \quad t = \frac{v_t^{\rm pp}}{\overline{v}_s^{\rm pair}}, \qquad (3.5)$$

where $\overline{v}_s^{\rm pair} = [v_s^{\rm pair}(p) + v_s^{\rm pair}(n)]/2$. In the pp channel the F (GT) excitations depend only on $s(t)$.

For the F excitations, and when the isospin nonconserving forces are absent, a self-consistent inclusion of the GSCs ($s = 1$) leads to the following: (i) the β^- strength $S_{\rm IAS}^+ \equiv S_0^{\{+1\}}$ is fully concentrated in the IAS, (ii) the β^+ strength $S_0^{\{-1\}}$, which in *pn*-QRPA can be viewed as an extension of the β^- spectrum to negative energies, is totally quenched, and (iii) the NME $M_F^{2\nu^-}(0_1^+)$ is null for all practical purposes. All this can be seen, for instance, from [[20], Figs. 1(b) and 1(c)], and [[47], Fig. 1]. The extent to which the above conditions are fulfilled at $s = s_{\rm sym} = 1$ may be taken as a measure of the isospin symmetry restoration.

For GT excitations, the GSCs lead to the following: (i) the β^- strength $S_1^{\{+1\}}$ is largely concentrated on the GT resonance, (ii) the β^+ strength $S_1^{\{-1\}}$ exhibits a pronounced minimum at $t \cong 1.2$, similar to that of $S_0^{\{-1\}}$ at $s = 1$, which is accordingly denominated $t_{\rm sym}$ (see [[20], Figs. 1(c) and 1(c′)]).

Thus, in *pn*-QRPA model the SU(4) symmetry is partially restored within the pp channel at minima of the strengths $S_0^{\{+1\}}$, and $S_1^{\{+1\}}$. For the residual interaction (3.1), this occurs at

$$s = s_{\rm sym} = 1, \quad \text{and} \quad t = t_{\rm sym} \cong 1.2. \qquad (3.6)$$

Briefly, the spin-isospin symmetry is partially restored within the *pn*-QRPA when the conditions (3.4) and (3.6) are met, and this restoration is the prerequisite for a physically adequate evaluation of the observables.

It has also been shown that in the vicinity of the place where the restoration is performed, the F and GT NMEs behave á la Padé [20,44–47], i.e.,

$$M_F^{2\nu^-}(s) = M_F^{2\nu^-}(s=0)\frac{1-s}{1-s_1}, \qquad (3.7)$$

with $s_1 > 1$ being the value of s where the *pn*-QRPA collapses for $J = 0$, and

$$M_{\rm GT}^{2\nu^-}(t) = M_{\rm GT}^{2\nu^-}(t=0)\frac{1-t/t_0}{1-t/t_1}, \qquad (3.8)$$

with $t_1 > t_0$, where t_0 and t_1 denote the zero and pole of this NME, respectively. In fact, for $J = 1$ the *pn*-QRPA collapses at $t = t_1$. Such behaviors can be visualized, for instance, from [[20], Figs. 1(b) and 1(b′)].

As noted before [47], in the *pn*-TDA, where the GSCs are neglected, the results for the observables are quite different, even if the self-consistence $s = 1$ is imposed. In fact, in this case, (i) the $S_0^{\{+1\}}$ strength is always fragmented, (ii) the perturbed $S_0^{\{-1\}}$, and $S_1^{\{-1\}}$ strengths remain equal to their unperturbed (BCS) values, and therefore have no minimums, and (iii) the NMEs are very large [$M_F^{2\nu^-}(0_1^+) = -0.107$, and $M_{\rm GT}^{2\nu^-}(0_1^+) = -0.663$] in comparison with those given in Ref. [[20], Table II], which are $M_F^{2\nu^-}(0_1^+) = -0.004$, and $M_{\rm GT}^{2\nu^-}(0_1^+) = 0.022$.

From the previous discussion it is clear that for the model developed here, we can use only the ph part (3.4) of the PSU4SR, namely (i) $v_s^{\rm ph} = 27$ and $v_t^{\rm ph} = 64$ for ^{48}Ca, and (ii) $v_s^{\rm ph} = 55$ and $v_t^{\rm ph} = 92$ for ^{96}Ru.

With respect to the pp parameters, we observe that the first relationship in Eq. (3.6) is always valid (both in the QRPA and QTDA models), since it is a consequence of the self-consistency between the pairing interaction $\overline{v}_s^{\rm pair}$, and the isovector pp interaction $v_s^{\rm pp}$. On the other hand, in the $(pn, 2p2n)$-QTDA there is no physical restriction on the isoscalar pp interaction $v_t^{\rm pp}$, therefore we will basically use

TABLE III. Calculated and measured NME (in natural units $\times 10^3$) for 2ν-DBDs of ^{48}Ca [$M^{2\nu}(\mathcal{J}_f^+) \equiv M^{2\nu^-}(\mathcal{J}_f^+)$] and ^{96}Ru [$M^{2\nu}(\mathcal{J}_f^+) \equiv M^{2\nu^+}(\mathcal{J}_f^+)$] to ground state 0_1^+, and first excited 0_2^+ and 2_1^+ states in the final nuclei ^{48}Ti and ^{96}Mo, respectively. Results from Refs. [18,58] for ^{48}Ca and from Refs. [9,14,59–61] for ^{96}Ru, as well as the experimental value for ^{48}Ca [1], are also shown in same units. Suhonen's results [9] correspond to those listed in his Table II for the channel $\alpha = 2e$.

	^{48}Ca				
Par	$M_F^{2\nu}(0_1^+)$	$M_{\rm GT}^{2\nu}(0_1^+)$	$\lvert M^{2\nu}(0_1^+)\rvert$	$\lvert M^{2\nu}(0_2^+)\rvert$	$\lvert M^{2\nu}(2_1^+)\rvert$
e_j					
$T1$	13	−53	40	13	0.64
$T2$	15	−62	47	16	0.69
$T3$	17	−75	58	20	0.75
$e_j^{\rm expt}$					
$T1$	18	−83	64	10	0.33
$T2$	21	−110	89	34	0.34
$T3$	24	−152	128	80	0.35
[18]			22		120
[58]			28	26	1.62
[1]			38 ± 3		
			^{96}Ru		
$T1$	0.13	−17	16	10	0.51
$T2$	0.15	−17	17	11	0.61
$T3$	0.17	−18	18	12	0.75
[9]			415–1437	492–1554	0.1–8.4
[14]			251		
[59]			101		
[60]			54		

$s = 1$, while the value of t, given in Eq. (3.6), will be taken only as a guide.

Moreover, instead of using the bare value $g_A = 1.27$ for the axial-vector coupling constant [55], we use an effective value $g_A = 1.0$.[7] Still smaller values for g_A have been used in the literature [57].

C. Nuclear matrix elements

We calculate simultaneously the NMEs $M_F^{2\nu}(0_f^+)$, $M_{\rm GT}^{2\nu}(0_f^+)$, $M^{2\nu}(0_f^+)$, and $M_{\rm GT}^{2\nu}(2_f^+)$ for all above mentioned $\mathcal{J}_f^+$ final states with the following three sets of pp parameters:

$$\begin{aligned} T1:&\ s = 1.00, \quad t = 0.80, \\ T2:&\ s = 1.00, \quad t = 1.00, \\ T3:&\ s = 1.00, \quad t = 1.20. \end{aligned} \tag{3.9}$$

In the upper part of Table III are shown the results for the decays $^{48}\text{Ca} \rightarrow {}^{48}\text{Ti}\ (0_1^+, 0_2^+, 2_1^+)$, evaluated with the two sets of spe drawn in Fig. 2. The results obtained by other authors [18,58], as well as the experimental value [1] of the NMEs, are shown below. The agreement between the calculated and measured results for $M^{2\nu}(0_1^+)$ can be considered satisfactory (in particular with spe e_j), taking into account that all nuclear parameters in the pp and ph channels are basically fixed, both for identical particles in H_{nn} and H_{pp}, and for nonidentical particles in H_{pn}. We hope that in the near future the NMEs $M^{2\nu}(0_2^+)$ and $M_{\rm GT}^{2\nu}(2_1^+)$ will also be measured.

Our results are consistent with the previous ones for all three decays. The NME $M^{2\nu}(0_1^+)$ has been calculated many times, but there are only a very few theoretical studies of $M^{2\nu}(0_2^+)$ and $M_{\rm GT}^{2\nu}(2_1^+)$. As far as we know, the first one of these has been evaluated only in Ref. [58], and the second one in Refs. [18,58] (see also Ref. [62]).

Table III shows that our F NMEs are not null, which is understandable since the current model does not consider the GSCs. To make them null, one has to go from $(pn, 2p2n)$-QTDA to $(pn, 2p2n)$-QRPA. This is a formidable task that we are planning to do next. Certainly, GSCs will also affect the results for other observables, whose scope is difficult to estimate at this time.

The present F NMEs are relatively small for both 0^+ levels, when compared with the corresponding GT ones, but in no way are they negligible. As seen in Eq. (2.1), these two NMEs always interfere destructively. It should be pointed out that the contributions of $M_F^{2\nu}(0_{f=1,2}^+)$ have not been considered in the just mentioned studies [18,58], therefore, strictly speaking, their results for $|M^{2\nu}(0_{f=1,2}^+)|$ should be compared with ours $|M_{\rm GT}^{2\nu}(0_{f=1,2}^+)|$.

It is interesting to note that the F NMEs are often omitted in the calculations, simply invoking isospin conservation. But, as explained above, this is a necessary but not sufficient condition for these NMEs to be null (see also the work of Satula *et al.* [63]).

An exception is the work of Šimkovic, Rodin, and Faessler [64], where partial restoration of isospin symmetry is achieved in the *pn*-QRPA, which leads to the disappearance of $M_F^{2\nu}$. This is accomplished by separating the renormalization parameter $g_{\rm pp}$ into isovector and isoscalar parts. The isovector parameter $g_{\rm pp}^{T=1}$ is chosen to be essentially equal to the pairing constant $g_{\rm pair}$, which is equivalent to our condition for self-consistency $s = 1$ [see also the Eq. (3.7)].

In the lower part of Table III the results for the $^{96}\text{Ru} \rightarrow {}^{96}\text{Mo}\ (0_1^+, 0_2^+, 2_1^+)$ decays are shown. The outcomes of previous calculations [9,14,59–61] are also presented. It is noticeable that the differences between our three calculations are much smaller than the differences with all the other works.

The discrepancies between the results for the NMEs presented in Table III come from the use of different nuclear models. For instance, in the study of the DBD$^+$ in ^{96}Ru, done by Suhonen [9], was used the multiple-commutator model (MCM), designed to connect states of the odd-odd nuclei to excited states of the neighboring even-even final nuclei [65]. In this model, the states in the odd-odd nucleus, as well as the final $\mathcal{J}_f^+ = 0_1^+$ state, are described in the standard way, i.e., by the *pn*-QRPA in the form (2.26), while excited states of the even-even nuclei are generated by the charge-conserving QRPA (cc-QRPA), described in detail in Ref. [24]. That is,

[7] This quenching is frequently attributed to the Δ-hole polarization effect on the axial-vector coupling constant [49]. Recently an explanation of the quenching of g_A within the context of effective field theories [56] has been presented.

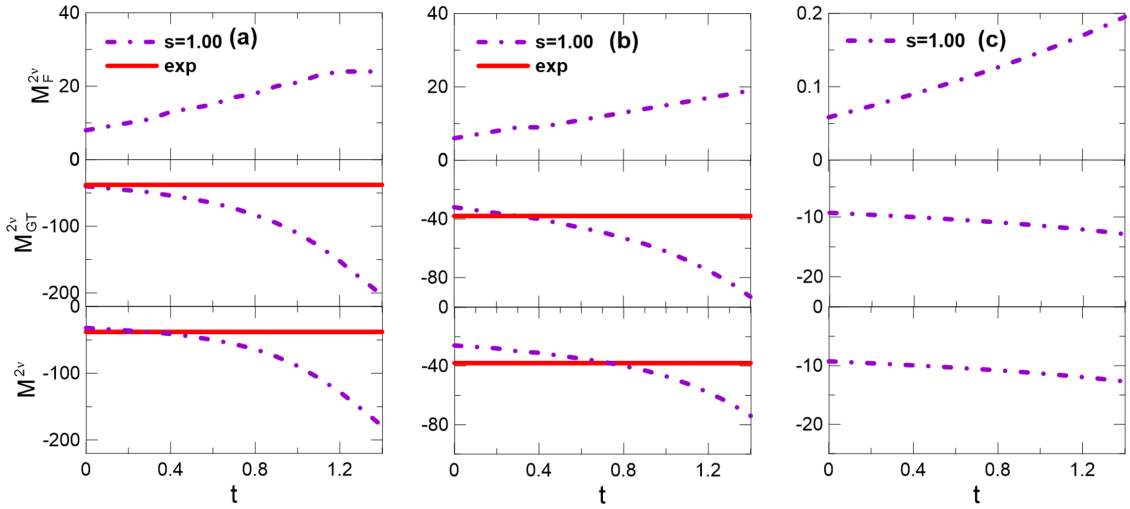

FIG. 3. Calculated NME $M_F^{2\nu}$, $M_{\rm GT}^{2\nu}$, and $M^{2\nu}$ for the ground 0^+ state (in natural units $\times 10^3$), as a function of the pp parameters t and s for ^{48}Ti for (a) ^{48}Ca with spe $e_j^{\rm expt}$, (b) ^{48}Ca with spe e_j, and (c) ^{96}Ru. The experimental value for ^{48}Ti $|M^{2\nu}(0_1^+)| = (38 \pm 3) \times 10^{-3}$ is also indicated by the red line, whose width represents the experimental error.

the final states $\mathcal{J}_f^+ = 2_1^+,\ 0_2^+,\ 2_3^+$, and 0_3^+ are assumed to be basic cc excitations (one-phonon cc-QRPA states), and the $\mathcal{J}_f^+ = 0_2^+$ and 2_2^+ states are considered as consisting of two 2_1^+ cc-QRPA phonons. Therefore, there is no physical similarity between the model used by Suhonen [9] and ours.

The strong dependence of the NME within the *pn*-QRPA model with respect to the isoscalar pp parameter t is well known and is often discussed, therefore, it could be interesting to analyze that dependence in the current model. This is done in Fig. 3 showing the NMEs $M_F^{2\nu}$, $M_{\rm GT}^{2\nu}$, and $M^{2\nu}$ for the ground 0^+ state in ^{48}Ca and ^{96}Ru, as a function of the pp parameters t and s. The experimental value of $|M^{2\nu}(0_1^+)|$ is also drawn. It can be concluded that within the present model such dependence is only moderate. The same statement is valid also for all remaining 2ν NMEs.

It is also well known that the relatively small values of the NME in the *pn*-QRPA model come from the destructive interference between forward and backward going contributions [20], that is, through the ground state correlations (GSCs). The quenching mechanism is different in the current model, and it is the consequence of the interplay between seniority-0 and seniority-4 configurations in the final states. For example, in the case of ^{48}Ca, within the space e_j and with force parameters $T1$, the NME $M^{2\nu}$ for the three lowest 0^+ states are $-0.040, -0.013, -0.040$. But, when only the seniority-0 configurations are considered, one finds $-0.068, -0.016, -0.065$, respectively, which confirms the above statement.

TABLE IV. Calculated half-lives $\tau_{2\nu}^{2\beta^-}(\mathcal{J}_f^+ = 0_1^+, 0_2^+, 2_1^+)$ (in units of yr) for the 2ν-DBD ^{48}Ca $\rightarrow$ ^{48}Ti. For the spe e_j, all three sets of the pp parameters, and with $g_A = 1$, are shown, and confronted with previous calculations and data. In Eq. (2.48) we use the $G_{2\nu}^{\alpha}(\mathcal{J}_f^+)$ factors from Ref. [66] for the levels $0_1^+ (=1.56 \times 10^{-17}\ \text{yr}^{-1})$ and $0_2^+ (=3.63 \times 10^{-22}\ \text{yr}^{-1})$, and from Ref. [67] for $2_1^+ (=4.41 \times 10^{-18}\ \text{yr}^{-1})$.

	0_1^+	0_2^+	2_1^+
$T1$	4.01×10^{19}	1.63×10^{25}	5.54×10^{23}
$T2$	2.90×10^{19}	1.08×10^{25}	4.76×10^{23}
$T3$	1.91×10^{19}	6.89×10^{24}	4.03×10^{23}
Ref. [18]			1.72×10^{24}
Ref. [58]	3.3×10^{19}		8.5×10^{23}
Expt. [1]	$(4.4^{+0.6}_{-0.5}) \times 10^{19}$		

D. Half-lives

Knowing the NMEs and the leptonic kinematic factors $G_{2\nu}^{\alpha}(\mathcal{J}_f^+)$, the corresponding half-lives $\tau_{2\nu}^{\alpha}(\mathcal{J}_f^+)$ are evaluated trivially from (2.48). Despite this, we present some of them only for the sake of completeness.

Our results for $\tau_{2\nu}^{2\beta^-}(\mathcal{J}_f^+ = 0_1^+, 0_2^+, 2_1^+)$ in ^{48}Ca, evaluated with spe e_j and the three sets of the pp parameters are compared with the previous calculations and with the data in Table IV. For the state 0_1^+ we agree both with the experiment [1] and with the SM calculation [58]. On the other hand, our half-life for the first 2_1^+ is shorter by a factor of about 2 than the same evaluated with SM [58], and by a factor of about 4 than the one obtained by Raduta *et al.* [18].

TABLE V. Calculated half-lives $\tau_{2\nu}^{\alpha}(\mathcal{J}_f^+ = 0_1^+)$ in units of yr for the 2ν-DBD ^{96}Ru $\rightarrow$ ^{96}Mo, with the pp parameter set $T2$ and $g_A = 1$ are shown and confronted with previous calculations. In Eq. (2.48) we use the $G_{2\nu}^{\alpha}(\mathcal{J}_f^+)$ factors from Ref. [17] for the channels $2\beta^+ (=1.080 \times 10^{-26}\ \text{yr}^{-1})$, $e\beta^+ (=0.454 \times 10^{-21}\ \text{yr}^{-1})$, and $2e (=2.740 \times 10^{-21}\ \text{yr}^{-1})$.

α	Present	[14]	[59]	[60]	[9]
$2\beta^+$	3.2×10^{29}	5.8×10^{26}		3.5×10^{28}	1.0×10^{27}
β^+e	7.6×10^{24}	1.2×10^{22}	8.6×10^{22}	9.1×10^{23}	2.3×10^{23}
ee	1.3×10^{24}	2.1×10^{21}	1.4×10^{22}	1.6×10^{23}	3.9×10^{21}

TABLE VI. Calculated $Q_{\beta\beta}$ and Q_{2e} values (in units of MeV) with the three sets of pp parameters $T1$, $T2$, and $T3$ and for the DCE processes: (a) ^{48}Ca → ^{48}Ti and ^{48}Ca → ^{48}Ar and (b) ^{96}Ru → ^{96}Mo and ^{96}Ru → ^{96}Pd are confronted with experiments.

		^{48}Ca	
	Par	$Q_{\beta\beta}$	Q_{2e}
$e_j^{\rm expt}$	$T1$	4.980	−20.673
	$T2$	5.300	−20.353
	$T3$	5.780	−19.872
e_j	$T1$	6.611	−15.835
	$T2$	6.710	−15.736
	$T3$	6.820	−15.626
Expt.		4.268	−21.943
		^{96}Ru	
e_j	$T1$	−7.728	3.266
	$T2$	−7.722	3.272
	$T3$	−7.715	3.279
Expt.		−9.896	2.714

In the case of ^{96}Ru, our results for the half-lives $\tau_{2\nu}^{\alpha}(0_1^+)$, for different decay modes ($\alpha = 2\beta^+, e\beta^+, 2e$), are shown in Table V. All of them are larger by one to three orders of magnitude when compared with previous theoretical studies, which are shown in the same table. The biggest discrepancies are in the *pn*-QRPA calculation made in Ref. [14]. The origin of what is difficult to elucidate given the difference between the two models used.

The experimental limits for the ^{96}Ru half-lives are $\tau_{2\nu}^{2\beta^+}(0_1^+) \geqslant 1.4 \times 10^{20}$ yr and $\tau_{2\nu}^{e\beta^+}(0_1^+) \geqslant 0.8 \times 10^{20}$ yr [68]. Thus, from Table V we see that our predictions are nine orders of magnitude larger for the $2\beta^+$ mode, and four orders of magnitude larger for the $e\beta^+$ mode. This, in turn, implies that the accuracy of the measurements would have to be significantly improved to observe these processes.

We have not evaluated the half-lives of the ^{96}Ru final states $\mathcal{J}_f^+ = 0_2^+, 2_1^+$, since their kinematic factors G^{α} are not available.

E. Q values and energy spectra

Before starting with the discussion of Q values, it is convenient to remember that a physical phenomenon is allowed only when this quantity is positive.

In Table VI the experimental data are confronted with our results for the $Q_{\beta\beta}$ and Q_{2e} values in the DCE processes: (a) ^{48}Ca → ^{48}Ti and ^{48}Ca → ^{48}Ar, and (b) ^{96}Ru → ^{96}Mo and ^{96}Ru → ^{96}Pd. One sees that the model is capable of reproducing fairly well not only the signs of the Q-values, but also their magnitudes, without having to modify the parameters of the model. This is very encouraging! In addition, it seems that the model "knows" what type of DCE decay can occur in a given nucleus.

The nature of Q value is predominantly determined by the proton and neutron pairing mean fields, as seen from (2.41) or, more precisely, from the relation $Q_{2e} - Q_{2\beta^-} = 4(\lambda_p - \lambda_n)$. The dependence on the residual interaction is rather weak and takes place through the ground state energy $\omega_{0_1^+}$ in the residual nuclei, as $Q_{2e} + Q_{2\beta^-} = -2\omega_{0_1^+}$. More details on how the Q-values depend on the pp coupling constants are shown in the Fig. 4.

As we stated before, in the same way that the *pn*-QRPA model [12] predicts identical energy spectra for odd-odd nuclei $(A, Z \pm 1)$, the present model predicts identical excitation energies in even-even nuclei $(A, Z \pm 2)$. This is obviously not realistic due to the large neutron excess.

It is pertinent to mention here that the use of particle-number-projection can become very important when working with the BCS mean-field [42]. Without a doubt, with this method different energy spectra are obtained in nuclei with the same mass number but different numbers of protons and neutrons.

But, despite the above-mentioned disadvantage, the predicted 0^+ and 2^+ excitation energies in ^{48}Ti and ^{48}Ar are consistent with the data, as shown in Fig. 5 for the spes $e_j^{\rm expt}$, e_j, and pp parametrization $T2$.

Because of the size of the $Q_{2\beta^-}$ value (= 4.268 MeV), the $2\beta^-$ decays are energetically possible for all states, except for the 0_4^+. We have evaluated the NMEs for all these states, but we do not consider it necessary to present them here. We have

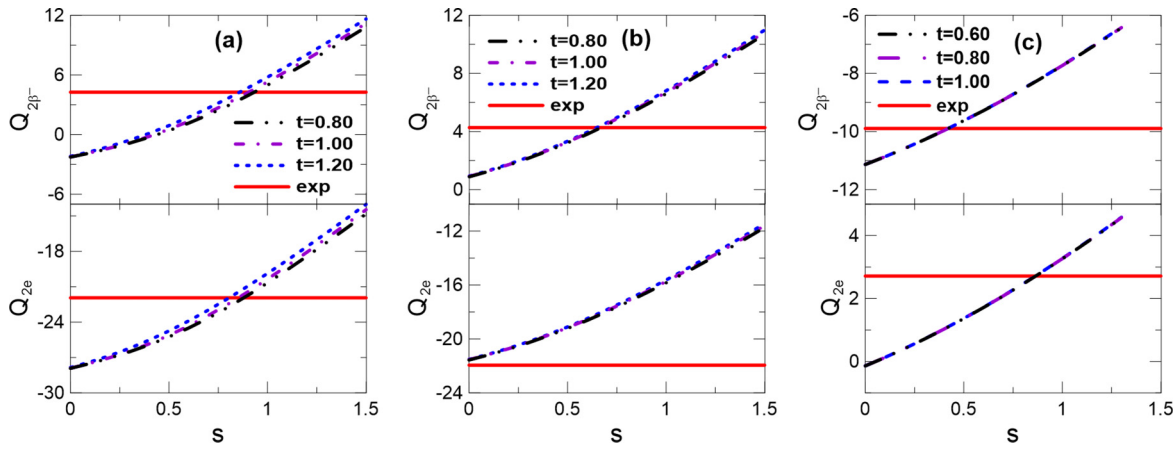

FIG. 4. Calculated $Q_{2\beta^-}$ and Q_{2e} values in ^{48}Ca with spe $e_j^{\rm expt}$ (a), and with spe e_j (b), and ^{96}Ru (c), as a function of pp parameters t and s. The experimental Q values are also shown.

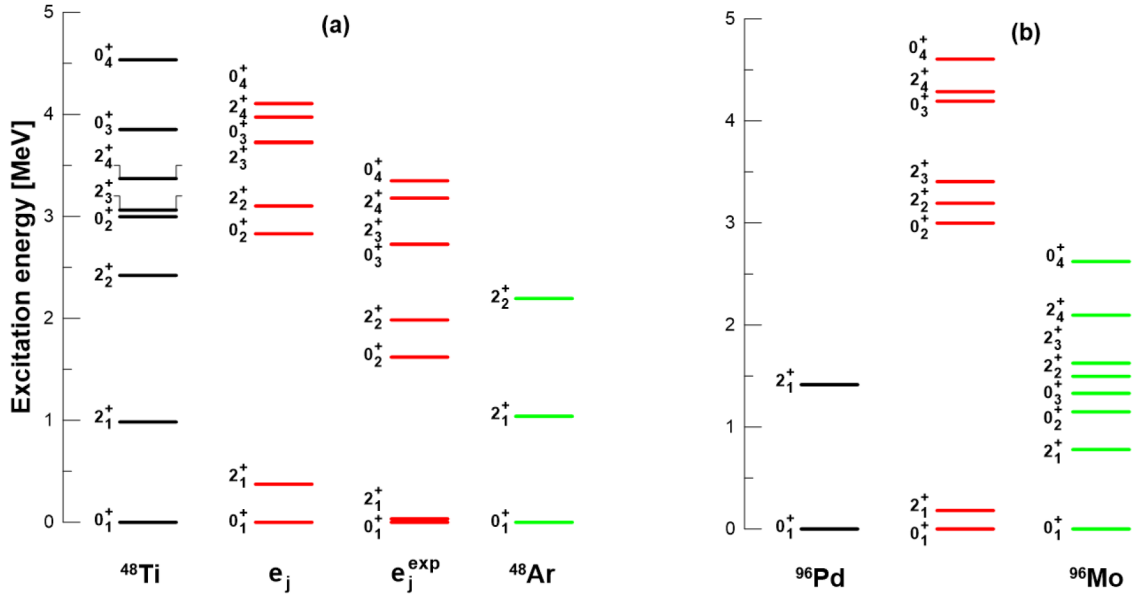

FIG. 5. (a) Experimental excitation energies of the final states $\mathcal{J}^\pi = 0^+$ and 2^+ are compared with calculations, performed with the pp parametrization $T2$, for (a) ^{48}Ti and ^{48}Ar and (b) ^{96}Pd and ^{96}Mo.

not found in the literature any detailed calculation of the low energy ^{48}Ti spectrum to compare with the ones obtained for us and shown in Fig. 5.

The experimental energy spectra of ^{96}Pd and ^{96}Mo are poorly explained by our calculations. However, for the sake of completeness, the comparison between theory and data is presented in Fig. 5(b). These two nuclei exhibit very different spectra from each other, and most likely no nuclear model explains their properties simultaneously, without dramatically varying the parameters of the model, which we do not do here. It is possible that GSCs significantly modify the energy spectra of final even-even nuclei, that is, when switching from $(pn, 2p2n)$-QTDA to $(pn, 2p2n)$-QRPA, as happens with the spectra of odd-odd nuclei when changing from pn-QTDA to pn-QRPA [24].

Excitation energies of ^{96}Mo are not evaluated in the MCM [9] as we do. What is done in the cc-QRPA model is to adjust the theoretical energies to the experimental ones, obtaining in this way the particle-hole channel parameters. This is carried out for each one-phonon state [65].

F. Double-charge-exchange strengths and their sum rules

The results for the DCE transition strengths $S^{\{\pm 2\}}_{J\mathcal{J}}$ given by (2.15), both for Fermi ($J = 0; \mathcal{J} = 0$) and Gamow-Teller ($J = 1; \mathcal{J} = 0, 2$) are displayed in Table VII. The corresponding sum rules $S^{\{2\}}_{J\mathcal{J}}$ calculated from (2.16) are also shown, and confronted with the predicted sum rules $\mathsf{S}^{\{2\}}_{J\mathcal{J}}$ given by (2.17)–(2.19). In addition, to know the locations of the DCE resonances, we have evaluated the energy centroid (2.50).

To obtain an idea of the magnitudes of the DBD, the strengths $B^{\{+2\}}_{J\mathcal{J}_1}$ ($B^{\{-2\}}_{J\mathcal{J}_1}$) going to the levels 0^+_1 and 2^+_1 in final ^{48}Ti (^{96}Mo) nucleus are explicitly given.

All calculations related to DCE transition strengths were performed for the three sets of pp parameters (3.9), finding that all produce identical results. We have also found that, at least in the case of ^{48}Ca, there is a certain dependence of the results with respect to the used spe spaces.

The results derived for ^{48}Ca within the SM for the pf space[8] by other authors are given in the last three bins of the upper part of Table VII—specifically, by (i) Sagawa and Uesaka [5] with GXFF1A interaction, and (ii) by Auerbach and Minh Loc [6] and Shimizu, Menéndez, and Yako [7], both with KB3G interaction. In fact, the values of strengths $S^{\{+2\}}_{1\mathcal{J}=0,2}$ attributed to the last authors [7] have been extracted from their Fig. 1(b).

Several observations are in order regarding the results shown in Table VII:

(1) The strengths $S^{\{-2\}}_{J\mathcal{J}}$ are always small in comparison with the strengths $S^{\{+2\}}_{J\mathcal{J}}$ and, as a consequence, $S^{\{+2\}}_{J\mathcal{J}} \cong \mathsf{S}^{\{2\}}_{J\mathcal{J}}$. This is clearly due to the relatively large neutron excess.

(2) Although small, the strengths $S^{\{-2\}}_{J\mathcal{J}}$ are significant in relation to the DBD. They are proportionally higher in ^{96}Ru, which decays by $2\beta^+$, than in ^{48}Ca, which decays by $2\beta^-$.

(3) The F strengths $S^{\{2\}}_{00}$ deviate quite significantly from the sum rule strengths $\mathsf{S}^{\{2\}}_{00}$—24% and 40%, respectively, within the spe spaces e^{expt}_j and e_j in ^{48}Ca,

[8]Note that the present calculations were done in a single-particle space consisting of the $2p$-$1f$-$2s$-$1d$ shells for both protons and neutrons.

TABLE VII. Results with the pp parametrization $T2$ for (i) Fermi ($J=0;\mathcal{J}=0$) and Gamow-Teller ($J=1;\mathcal{J}=0,2$) DCE transition strengths $S^{\{\pm2\}}_{J\mathcal{J}}$ given by (2.15), (ii) the corresponding sum rules $S^{\{2\}}_{J\mathcal{J}}$ calculated from (2.16), (iii) the predicted sum rules $\mathsf{S}^{\{2\}}_{J\mathcal{J}}$ given by (2.17)–(2.19), (iv) the energy centroid (2.50), and (v) the transition strengths $B^{\{2\}}_{J\mathcal{J}_1}(\equiv B^{\{+2\}}_{J\mathcal{J}_1})$ for ^{48}Ca and $B^{\{2\}}_{J\mathcal{J}_1}(\equiv B^{\{-2\}}_{J\mathcal{J}_1})$ for ^{96}Ru going to the levels 0^+_1 and 2^+_1. The SM results from previous works [5–7] for ^{48}Ca are also shown. The meaning of the inequalities is explained in the text.

		^{48}Ca						
Ref.	$J\mathcal{J}$	$S^{\{+2\}}_{J\mathcal{J}}$	$S^{\{-2\}}_{J\mathcal{J}}$	$S^{\{2\}}_{J\mathcal{J}}$	$\mathsf{S}^{\{2\}}_{J\mathcal{J}}$	$\bar{E}^{\{-2\}}_{00}$	$\bar{E}^{\{+2\}}_{00}$	$10^3 B^{\{2\}}_{J\mathcal{J}_1}$
	00	140.1	0.94	139.1	112	21.7	17.61	177
e^{expt}_j	10	162.2	2.0	160.2	$\leqslant$175.9	13.0	17.60	1060
	12	716.1	9.10	707.0	$\geqslant$639.6	14.4	17.88	86.1
	00	157.2	2.4	154.8	112	22.0	22.6	95.6
e_j	10	189.9	5.9	184.0	$\leqslant$198.6	14.3	17.5	389
	12	859.3	26.0	833.3	$\geqslant$753.2	15.2	17.7	93.1
[5]	10			135.5	$\leqslant$144.0			
	12			501.2	$\geqslant$480.0			
[6]	10	131.8			$\leqslant$144.0	21.9		24.0
[7]	10	126.3						
	12	511.0						
		^{96}Ru						
	00	128.0	0.1	127.9	112	21.3	19.9	0.005
e_j	10	221.1	12.0	209.1	$\leqslant$222.7	23.0	12.4	4.1
	12	981.4	49.0	932.4	$\geqslant$873.5	23.2	11.8	11.1
[61]	00							0.000
	10							1570

and 14% in ^{96}Ru. A possible explanation for these differences is given in the Appendix.[9]

(4) Terms proportional to C in the GT sum rules Eqs. (2.18)–(2.20) are not included in the calculations, and this is the reason why the following conditions must be fulfilled:

$$S^{\{2\}}_{10} \leqslant \mathsf{S}^{\{2\}}_{10},$$
$$S^{\{2\}}_{12} \geqslant \mathsf{S}^{\{2\}}_{12}. \tag{3.10}$$

In fact, they are nicely satisfied in all numerical calculations presented in Table VII.

(5) All $S^{\{\pm2\}}_{J\mathcal{J}}$ strengths depend quite significantly on the spe, but very weakly on the residual interaction. This is the reason why we only show the results for the parametrization $T2$.

(6) The same situation applies to the predicted sum rules $\mathsf{S}^{\{2\}}_{1\mathcal{J}}$, due to their dependence on the term $S^{\{-1\}}_1$ [in Eqs. (2.18)–(2.20)], which in turn depends on the spe used in the calculations.

(7) The terms proportional to $S^{\{-1\}}_1$ in Eqs. (2.18) and (2.19) are omitted in Refs. [5,6], and this is the reason why their predicted sum rules $\mathsf{S}^{\{2\}}_{1\mathcal{J}}$ are smaller than ours.

(8) Since the values for $S^{\{+2\}}_{1\mathcal{J}}$ are not explicitly given in Shimizu *et al.* [7], we have derived them from their Fig. 1(b). They are consistent with the values of $\mathsf{S}^{\{2\}}_{1\mathcal{J}}$ presented in Refs. [5,6].

(9) Our GT strengths are always larger than those in the SM calculations. Also, our average energies $\bar{E}^{\{+2\}}_{1\mathcal{J}}$ are significantly smaller than those presented in Table II in Ref. [6], and those shown in Fig. 1(b) by Shimizu *et al.* [7]. It is difficult to discern whether this is due to the deficiency of our model, or the difference in the size of the single-particle spaces. We are inclined to think that our results are correct, since, otherwise, it would be very difficult to satisfy the second condition in Eq. (3.10), when in Eq. (2.19) is considered the strength $S^{\{-1\}}_1$.

(10) From the comparison of the transition strengths $B^{\{\pm2\}}_{J\mathcal{J}_1}$, corresponding to the states $\mathcal{J}^+_1=0^+_1$, and 2^+_1, with total strengths $S^{\{\pm2\}}_{J\mathcal{J}}$, we can get an idea of how small the NMEs are.

(11) The correspondence between F and GT NMEs, defined in Ref. [[61], Eq. (15)], and our $B^{\{+2\}}_{J=0,1,0}$ densities is

$$\left|M^{(2\nu)}_{\text{F}}\right|^2 \to B^{\{+2\}}_{0,0},$$
$$\left|M^{(2\nu)}_{\text{GT}}\right|^2 \to 3B^{\{+2\}}_{1,0}. \tag{3.11}$$

G. Spectral distributions of double-charge-exchange strengths

The DCE strength distributions $B^{\{\pm2\}}_{J\mathcal{J}_f}$, which are of interest here, are drawn in Figs. 6–8 as a function of the excitation energy $\mathcal{E}$ in the final nuclei. We have found that they depend only moderately on the spe spaces, and even less on the pp parameters. To simulate the experimental energy resolution, they were smeared out with Lorentzians of 1 MeV width. Moreover, these figures contain inserts which show the corresponding strengths in the low-lying states of the final nuclei.

The F distribution $B^{\{+2\}}_{00}$ in ^{48}Ti, shown in the upper panel of Fig. 6, exhibits at around 22 MeV a fairly narrow resonance, usually called a double isobaric analog state (DIAS). In the middle and lower panels of this figure are shown the GT distributions $B^{\{+2\}}_{10}$ and $B^{\{+2\}}_{12}$, respectively, in the same final nucleus, which also exhibit resonantlike structure. These double GT giant resonances (DGTGRs) are much wider than the DIAS and centered around 13 and 14 MeV, respectively. In the KB3G SM calculations of Shimizu *et al.* [7], which are also shown in Fig. 6, these resonances appear at around 20 MeV.

Analogous results for the $B^{\{+2\}}_{J\mathcal{J}}$ and $B^{\{-2\}}_{J\mathcal{J}}$ densities in ^{96}Pd and ^{96}Mo, respectively, are presented in Figs. 7 and 8. Both results are shown because here we are interested in the DBD^+, where the low-energy behavior of $B^{\{-2\}}_{J\mathcal{J}}$ densities is relevant.

[9] In this case it could be interesting to analyze if the problem can be solved by particle-number projection [42].

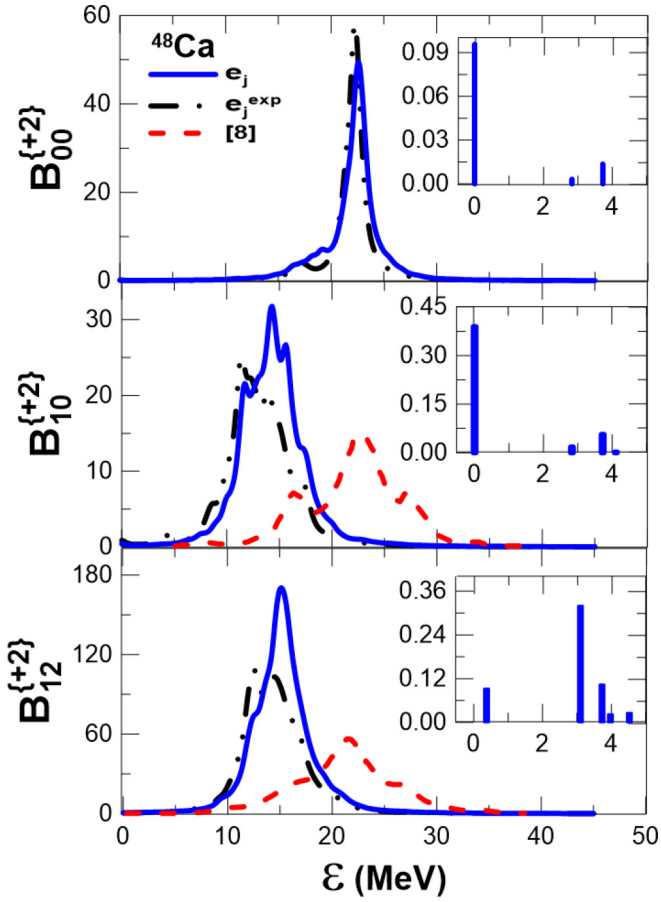

FIG. 6. DCE strength distributions $B^{\{+2\}}_{J\mathcal{J}}$ for the transition ^{48}Ca $\rightarrow$ ^{48}Ti with spe e_j, and $e^{\rm expt}_j$, and pp strengths $T2$, as a function of the excitation energy $\mathcal{E}$ in ^{48}Ti. The $B^{\{+2\}}_{J\mathcal{J}}$ are dimensionless, and the energies are in MeV. The SM results, obtained by Shimizu *et al.* [7] with the KB3G interaction, are also shown.

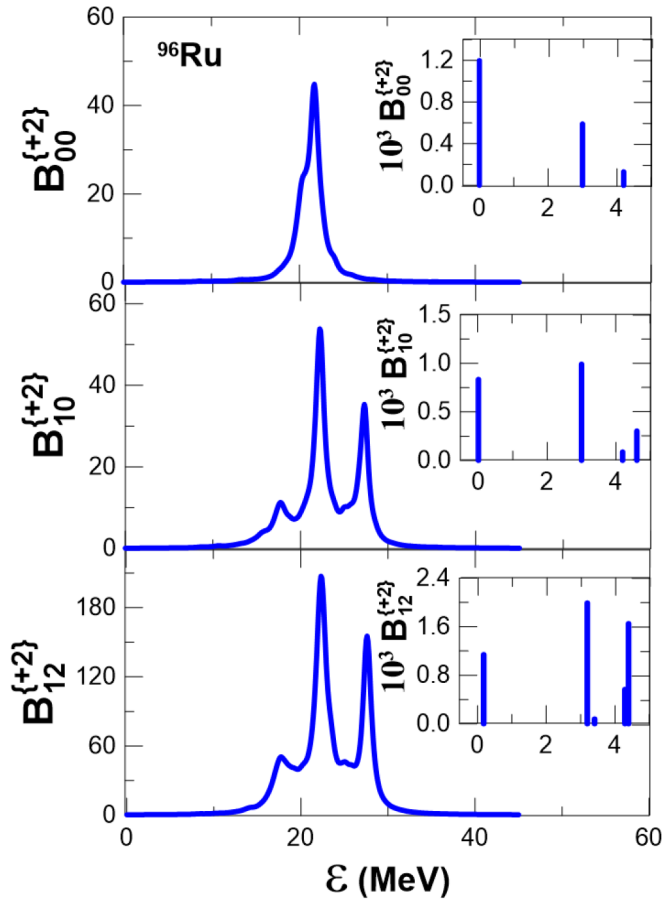

FIG. 7. DCE strength distributions $B^{\{+2\}}_{J\mathcal{J}}$ for the transition ^{96}Ru $\rightarrow$ ^{96}Pd with pp strengths $T2$ as a function of the excitation energy $\mathcal{E}$ in ^{96}Pd. The $B^{\{+2\}}_{J\mathcal{J}}$ are dimensionless, and the energies are in MeV.

As seen in Fig. 7, the DIAS in ^{96}Pd is located at around 21 MeV, while both $\mathcal{J} = 0^+$ and $\mathcal{J} = 2^+$ DGTGRs are at about 23 MeV. These resonances are not directly related to the DBD of ^{96}Ru, but their locations in ^{96}Pd can be searched through heavy ion reactions.

The smallness of $B^{\{-2\}}_{00}$ and its energy distribution, shown in Fig. 8, are fully consistent with the small value of $M^{2\nu}_F(0^+_1)$ in Table III and of $B^{\{-2\}}_{00_1}$ in Table VII. Moreover, the distributions of the $B^{\{-2\}}_{1\mathcal{J}=0,2}$ clearly indicate that the DBD$^+$ of ^{96}Ru will be very slow.

The role played by the residual interaction in generating DIAS is illustrated in Fig. 9, where a few results for the F distribution $B^{\{+2\}}_{00}$ in ^{48}Ti are exhibited. Panel (a) shows how the unperturbed (BCS) strength moves upwards in energy by about 15 MeV, due to the residual interaction in the ph channel. In panel (b), the F distributions are shown when the full residual interaction acts, with $t = 1$, and several different values of s. The maximum concentration of strength occurs for $s = 1$ at around 22 MeV, thus generating the double isobaric analogous state (DIAS). This, in turn, clearly shows the importance of the self-consistency ($s = 1$) between the pairing force and the pp isovector interaction.

But, as seen from the insert in the panel (b), not all the double F strength is contained in a single state. If this would happen after moving from the QTDA to the QRPA, and thus completely reset the spin-isospin symmetry, it remains an open question.

H. Comparison between ground state 2ν-DBD NME and DCE strengths

In the so-called closure approximation is used the completeness character of the intermediate states $|J_\alpha\rangle$ in Eqs. (2.1) and (2.9), after replacing the energies $E^{\{\mp 1\}}_{J_\alpha}$ in Eq. (2.3) by some average $\bar{E}^{\{\mp 1\}}_J$ [67].

Thus, except for the constant energy denominator, the ground state DCE densities $B^{\{\pm 2\}}_{J0_1}$ are the closure approximations of the squares of the NMEs. In view of this, to know how reasonable the closure approximation is, it may be interesting to compare the behaviors of these two quantities as a function of the pp parameters.

As an example, in Fig. 10 we compare $|M^{2\nu}_{\rm F}(0^+_1)|^2$ and $|M^{2\nu}_{\rm GT}(0^+_1)|^2$ with $B^{\{+2\}}_{00_1}$ and $B^{\{+2\}}_{10_1}$, respectively, evaluated in

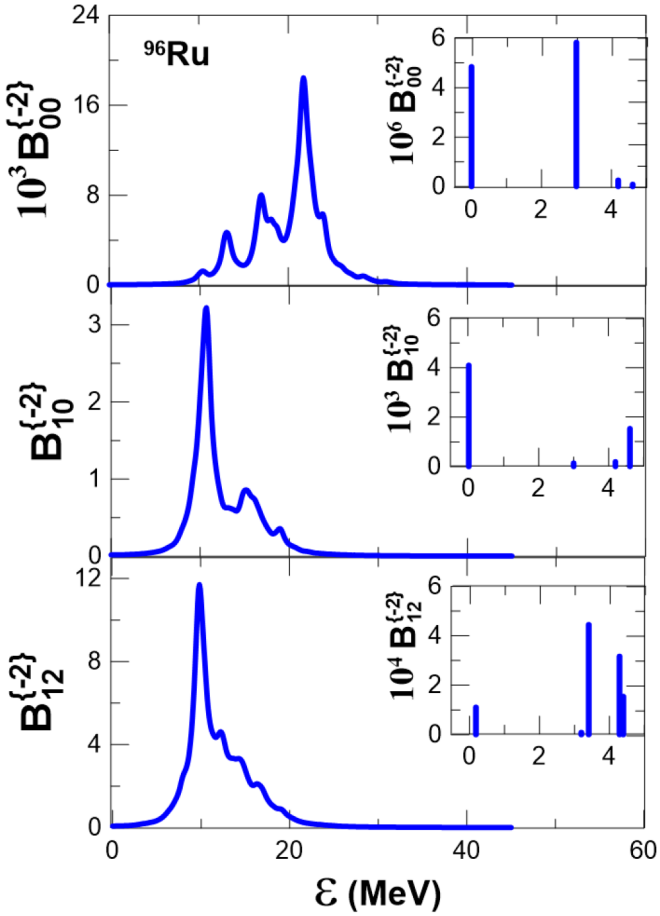

FIG. 8. DCE strength distributions $B^{\{-2\}}_{J\mathcal{J}}$ for the transition ^{96}Ru $\rightarrow$ ^{96}Mo. with pp strengths $T2$ as a function of the excitation energy $\mathcal{E}$ in ^{96}Mo. The $B^{\{-2\}}_{J\mathcal{J}}$ are dimensionless, and the energies are in MeV.

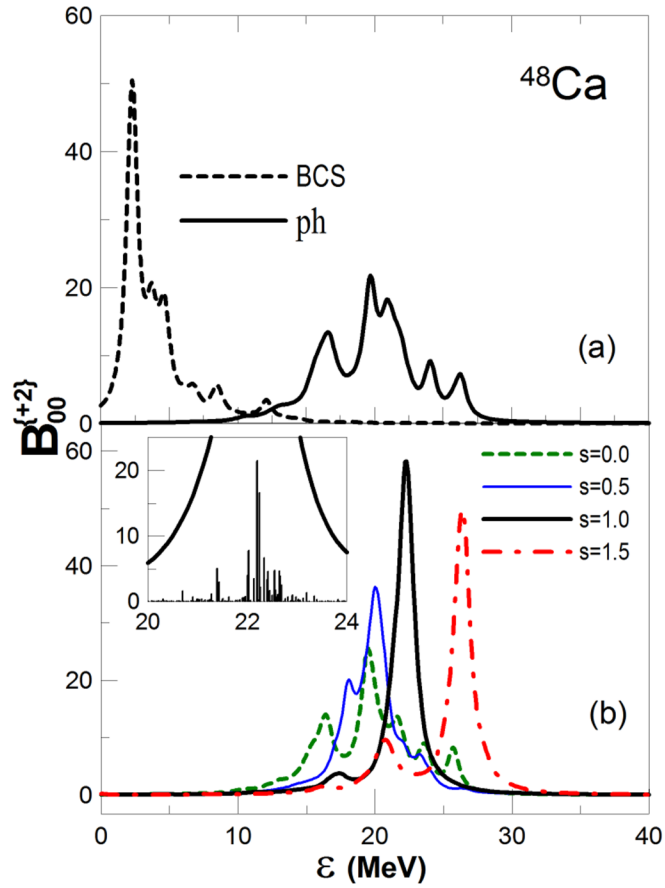

FIG. 9. DCE strength distributions $B^{\{+2\}}_{00}$ for the transition ^{48}Ca $\rightarrow$ ^{48}Ti with spe e^{expt}_j, for several parametrizations of the residual interaction. The inserted figure in (b) shows the splitting of the double F strength within the DIAS. See text for details.

^{48}Ca with the spe e_j. The squares of the NMEs are in natural units, while the strengths are dimensionless. The proportionality between these two observables suggests that the closure approximation in the case of ^{48}Ca is reasonable. However, there is no guarantee that this result will be valid i n general.

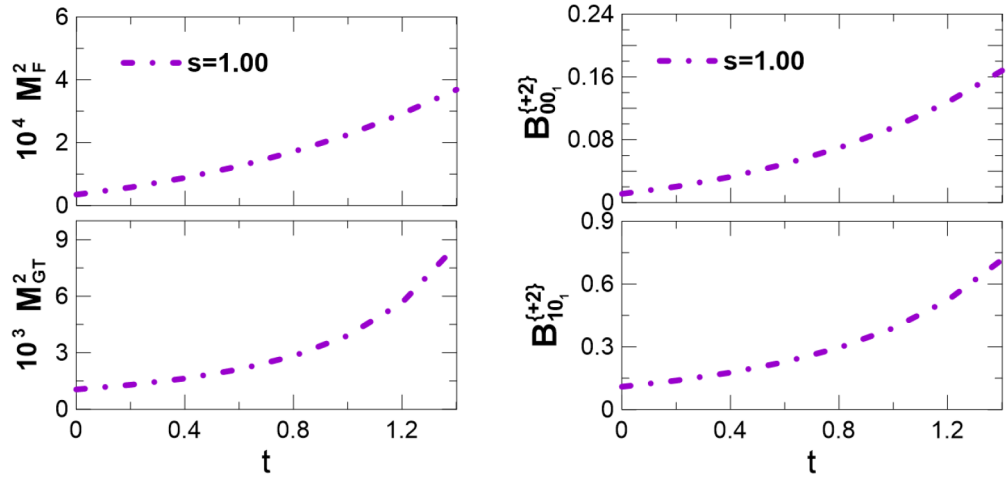

FIG. 10. Comparison of $|M^{2\nu}_F(0^+_1)|^2$ and $|M^{2\nu}_{\text{GT}}(0^+_1)|^2$ (both in natural units) with $B^{\{+2\}}_{00_1}$ and $B^{\{+2\}}_{10_1}$ (dimensionless), respectively, in ^{48}Ca for the spe e_j.

IV. FINAL REMARKS

We have developed a nuclear structure model that involves $(pn, 2p2n)$-QTDA excitations on the BCS mean field, which is capable of simultaneously describing the DBD and the DCE transition strengths. So far, this has been done only in the context of SM, where these two problems are generally treated separately, although it is well known that they are intimately related to each other. This is the case, for instance, of ^{48}Ca, where the DBD$^-$s are described in Refs. [18,58], while the transition strength distributions $B^{\{+2\}}_{J\mathcal{J}}$ and the corresponding total strengths $S^{\{+2\}}_{J\mathcal{J}}$ were evaluated in Refs. [5–7].

The $(pn, 2p2n)$-QTDA model has additional advantages over the standard pn-QRPA model, namely:

(1) Together with the NMEs of the ground state, the NMEs of all the excited states 0^+ and 2^+ are calculated simultaneously. In order to do the same in the pn-QRPA model, it is necessary to resort to supplementary calculations through several charge-conserving QRPAs, thus introducing several new model parameters.
(2) It allows the evaluation of the Q values for DBDs, which play a very important role in these types of processes.

The $(pn, 2p2n)$-QTDA aims to describe the DCE processes and is the natural extension of pn-QRPA, developed by Halbleib and Sorensen [12] to describe the SCE processes. However, the first model, unlike the second, does not include ground state correlations, which play a central role within the pn-QRPA to reduce NMEs. To include this type of correlation at the level of $2p2n$ excitations, it is necessary to go from $(pn, 2p2n)$-QTDA to $(pn, 2p2n)$-QRPA.

It should be borne in mind that, in the same way as the pn-QRPA put into play the seniority-4 configurations, the $(pn, 2p2n)$-QRPA will induced the seniority-6 and -8 configurations, which could be relevant in the evaluation of NMEs, such as are in the shell model calculations [69,70].

Our next aim is to evaluate and discuss the 0ν-NMEs (2.12) making use of the replacement (2.11) in our previous work [20]. One expects that the relationship between DCE nuclear reactions and DBD will be more clearly visible at 0ν decays than at 2ν decays, due to a lower dependence on the NME of their energy denominators than in the first case.

During the development of the present study, Santopinto *et al.* [71], based on a previous work of Bertulani [72], have reported that, in the low-momentum-transfer limit, the heavy ion ^{40}Ca(^{18}O, ^{18}Ne)^{40}Ar cross section behaves as

$$\frac{d\sigma}{d\Omega} \sim \left| \frac{\mathcal{M}^{\rm DGT}_{T\to T'}\mathcal{M}^{\rm DGT}_{P\to P'}}{\bar{E}^{\rm GT}_P + \bar{E}^{\rm GT}_T} + \frac{\mathcal{M}^{\rm DF}_{T\to T'}\mathcal{M}^{\rm DF}_{P\to P'}}{\bar{E}^{\rm F}_P + \bar{E}^{\rm F}_T} \right|^2,$$

where P and T stand for projectile and target nuclei respectively.

The correspondence with our notation is as follows:

(1) For the matrix elements[10]

$$\mathcal{M}^{\rm DGT}_{P\to P'} \to B^{\{+2\}}_{10_1}, \quad \mathcal{M}^{\rm DF}_{P\to P'} \to B^{\{+2\}}_{00_1},$$
$$\mathcal{M}^{\rm DGT}_{T\to T'} \to B^{\{-2\}}_{10_1}, \quad \mathcal{M}^{\rm DF}_{T\to T'} \to B^{\{+2\}}_{00_1}.$$

(2) For the energies [see the denominator in Eq. (2.2)]

$$E^{\rm GT}_P \to E^{\{+1\}}_{1_\alpha} - E^{\{0\}}_{0^+}, \quad E^{\rm F}_P \to E^{\{+1\}}_{0_\alpha} - E^{\{0\}}_{0^+},$$
$$E^{\rm GT}_T \to E^{\{-1\}}_{1_\alpha} - E^{\{0\}}_{0^+}, \quad E^{\rm F}_T \to E^{\{-1\}}_{0_\alpha} - E^{\{0\}}_{0^+}.$$

Therefore, the present model possesses all the necessary ingredients to evaluate the heavy-ion cross section in the low-momentum-transfer limit. Of course, now it is necessary to solve two eigenvalue problems, one for the target nucleus ^{40}Ca, and one for the projectile nucleus ^{18}O.

In summary, we have developed a new model, based on the BCS approach, to describe the double-charge-exchange nuclear phenomena $(A, Z) \to (A, Z \pm 2)$. It is a natural extension of the Halbleib and Sorensen [12] model, aimed to describe the single-charge exchange processes $(A, Z) \to (A, Z \pm 1)$. As an example, detailed numerical calculations are presented for the $(A, Z) \to (A, Z + 2)$ process in ^{48}Ca $\to$ ^{48}Ti and the $(A, Z) \to (A, Z - 2)$ process in ^{96}Ru $\to$ ^{96}Mo, involving several final 0^+ and 2^+ states. At the moment we are extending this study in three directions:

(1) A thorough evaluation of all 2ν- DBD$^\pm$, together with the associated nuclear reaction strengths will be performed.
(2) The 2ν- DBD$^\pm$ formalism developed here will be extended to the 0ν- DBD$^\pm$.
(3) The $(pn, 2p2n)$-QTDA model will be extended to the $(pn, 2p2n)$-QRPA model.

ACKNOWLEDGMENTS

This study was financed in part by the Coordenação de Aperfeiçoamento de Pessoal de Nível Superior Brasil (CAPES) Finance Code 001. A.R.S. acknowledges the financial support of FAPESB (Fundação de Amparo à Pesquisa do Estado Bahia) TERMO DE OUTORGA-PIE0013/2016. The authors thank the partial support of UESC (PROPP 00220.1300.1832). We sincerely thank W. Seale for his very careful and judicious reading of the manuscript. A.R.S. thanks G. Goldberg for reading the manuscript. We also thank N. Paar for providing us the spe for ^{96}Ru, evaluated within the (DD-ME2) model, and C. Bertulani and C. Barbero for stimulating comments and discussions.

APPENDIX: TOY MODEL

In order to understand why F DCESR is not completely satisfied in our model, we resort to a toy model corresponding to the ^{14}C nucleus and considering the levels $1s_{1/2}$, $1p_{1/2}$, and $1p_{3/2}$, of which the three are totally occupied by neutrons,

[10]Except for the coupling constants $c_{\rm GT}$ and $c_{\rm GT}$ in their Eqs. (11) and (12).

while only the first two are partially occupied by protons. From (2.15) we have

$$S_{00}^{\{-2\}} = \sum_f B_{00_f}^{\{-2\}} = \sum_f \left| \sum_\alpha \langle 0_f^+ || \mathcal{O}_0^- || 0_\alpha^+ \rangle \langle 0_\alpha^+ || \mathcal{O}_0^- || 0_i^+ \rangle \right|^2 . \tag{A1}$$

In the BCS approximation, one obtains

$$B_{00_1}^{\{-2\}} = 4u_{1p_{1/2}}^4, \quad B_{00_2}^{\{-2\}} = 4u_{1s_{1/2}}^2 u_{1p_{1/2}}^2,$$
$$B_{00_3}^{\{-2\}} = 12u_{1s_{1/2}}^2 u_{1p_{1/2}}^2, \quad B_{00_4}^{\{-2\}} = 4u_{1s_{1/2}}^4,$$

and

$$S_{00}^{\{-2\}} \equiv S_F^{2\beta^-} = 4 + 8u_{1s_{1/2}}^2 u_{1p_{1/2}}^2, \tag{A2}$$

since $u_{1s_{1/2}}^2 + u_{1p_{1/2}}^2 = 1$. For instance, with $u_{1s_{1/2}}^2 = 0.95$ and $u_{1p_{1/2}}^2 = 0.05$, one gets $S_{00}^{\{-2\}} = 4.382$, instead of the predicted value $S_{00}^{\{-2\}} = 4$. The result (A2) is also valid when the residual interaction is switched on. This means that the F DCESR is fully satisfied only in the particle-hole limit, i.e., when one of the protons' $1s_{1/2}$, $1p_{1/2}$ levels is totally full or totally empty.

[1] A. S. Barabash, Nucl. Phys. A **935**, 52 (2015).
[2] F. Cappuzzello, M. Cavallaro, C. Agodi, M. Bondi, D. Carbone, A. Cunsolo, and A. Foti, Eur. Phys. J. A **51**, 145 (2015).
[3] D. Carbone *et al.*, J. Phys. Conf. Ser. **1078**, 012008 (2018)
[4] H. Lenske, F. Cappuzzello, M. Cavallaro, and M. Colonna, Prog. Part. Nucl. Phys. **109**, 103716 (2019).
[5] H. Sagawa and T. Uesaka, Phys. Rev. C **94**, 064325 (2016).
[6] N. Auerbach and B. M. Loc, Phys. Rev. C **98**, 064301 (2018).
[7] N. Shimizu, J. Menéndez, and K. Yako, Phys. Rev. Lett. **120**, 142502 (2018).
[8] A. Escuderos, A. Faessler, V. Rodin, and F. Simkovic, J. Phys. G **37**, 125108 (2010).
[9] J. Suhonen, Phys. Rev. C **86**, 024301 (2012).
[10] D. S. Delion and J. Suhonen, Phys. Rev. C **95**, 034330 (2017).
[11] F. Krmpotić, Fizika B **14**, 139 (2005).
[12] J. A. Halbleib and R. A. Sorensen, Nucl. Phys. A **98**, 542 (1967).
[13] C. Barbero, F. Krmpotić, and A. Mariano, Phys. Lett. B **345**, 192 (1995).
[14] M. Hirsch, K. Muto, T. Oda, and H. V. Klapdor-Kleingrothaus, Z. Phys. A: Hadrons Nucl. **347**, 151 (1994).
[15] J. P. Pirinen and J. Suhonen, Phys. Rev. C **91**, 054309 (2015).
[16] H. Li and Z. Ren, Phys. Rev. C **96**, 065503 (2017).
[17] M. Doi and T. Kotani, Prog. Theor. Phys. **87**, 1207 (1992).
[18] A. A. Raduta and C. M. Raduta, Phys. Lett. B **647**, 265 (2007).
[19] A. Shukla, R. Sahu, and V. K. B. Kota, Phys. Rev. C **80**, 057305 (2009).
[20] V. dos S. Ferreira, F. Krmpotić, C. A. Barbero, and A. R. Samana, Phys. Rev. C **96**, 044322 (2017).
[21] P. Vogel, M. Ericson, and J. D. Vergados, Phys. Lett. B **212**, 259 (1988).
[22] K. Muto, Phys. Lett. B **277**, 13 (1992).
[23] D. C. Zheng, L. Zamick, and N. Auerbach, Phys. Rev. C **40**, 936 (1989).
[24] J. Suhonen, *From Nucleons to Nucleus: Concepts of Microscopic Nuclear Theory* (Springer, Berlin, 2007).
[25] M. K. Pal, Y. K. Gambhir, and R. Raj, Phys. Rev. **155**, 1144 (1966).
[26] R. Raj and M. L. Rustgi, Phys. Rev. **178**, 1556 (1969).
[27] M. Baranger, Phys. Rev. **120**, 957 (1960).
[28] J. Hirsch and F. Krmpotíc, Phys. Rev. C **41**, 792 (1990).
[29] A. R. Samana, F. Krmpotić, and C. A. Bertulani, Comput. Phys. Commun. **181**, 1123 (2010).
[30] A. Bohr and B. R. Mottelson, in *Nuclear Structure* (W. A. Benjamin, New York, 1969), Vol. 1.
[31] J. Kotila and F. Iachello, Phys. Rev. C **87**, 024313 (2013).
[32] S. Stoica and M. Mirea, Front. Phys. **7**, 12 (2019).
[33] S. Stoica, Chin. Phys. C **43**, 064108 (2019).
[34] N. Schwierz, I. Wiedenhover, and A. Volya, arXiv:0709.3525 [nucl-th].
[35] M. Kortelainen *et al.*, Phys. Rev. C **89**, 054314 (2014).
[36] C. Conci, V. Klemt, and J. Speth, Phys. Lett. B **148**, 405 (1984).
[37] F. Krmpotić, A. Samana, and A. Mariano, Phys. Rev. C **71**, 044319 (2005).
[38] R. Almar, O. Civitarese, and F. Krmpotić, Phys. Rev. C **8**, 1518 (1973).
[39] V. Paar, Nucl. Phys. A **211**, 29 (1973).
[40] N. Paar (private communication).
[41] N. Paar, D. Vretenar, T. Marketin, and P. Ring, Phys. Rev. C **77**, 024608 (2008).
[42] F. Krmpotić, A. Mariano, T. T. S. Kuo, and K. Nakayama, Phys. Lett. B **319**, 393 (1993).
[43] F. Krmpotić, in *Proceedings of the Lectures on Hadron Physics* (World Scientific, Singapore, 1990), p. 205.
[44] F. Krmpotić, J. Hirsch, and H. Dias, Nucl. Phys. A **542**, 85 (1992).
[45] F. Krmpotić, Phys. Rev. C **48**, 1452 (1993).
[46] F. Krmpotić, Rev. Mex. Fís. Sup. **40**, 285 (1994).
[47] F. Krmpotić and S. S. Sharma, Nucl. Phys. A **572**, 329 (1994).
[48] K. Nakayama, A. Pio Galeão, and F. Krmpotić, Phys. Lett. B **114**, 217 (1982).
[49] G. E. Brown and M. Rho, Nucl. Phys. A **372**, 397 (1981); A. Bohr and B. R. Mottelson, Phys. Lett. B **100**, 10 (1981); H. Castillo and F. Krmpotić, Nucl. Phys. A **469**, 637 (1987).
[50] S. Yoshida, Y. Utsuno, N. Shimizu, and T. Otsuka, Phys. Rev. C **97**, 054321 (2018).
[51] D. J. Thouless, Nucl. Phys. **22**, 78 (1960).
[52] C. A. Engelbrecht and R. H. Lemmer, Phys. Rev. Lett. **24**, 607 (1970).
[53] H. C. Lee, Phys. Rev. Lett. **27**, 200 (1971).
[54] A. M. Lane and J. Martorell, Ann. Phys. **129**, 273 (1980).
[55] J. Beringer *et al.* (Particle Data Group), Phys. Rev. D **86**, 010001 (2012).
[56] P. Gysbers *et al.*, Nat. Phys. **15**, 428 (2019).
[57] J. T. Suhonen, Front. Phys. **5**, 55 (2017); J. Suhonen, J. Phys.: Conf. Ser. **1056**, 012056 (2018).
[58] M. Horoi, S. Stoica, and B. A. Brown, Phys. Rev. C **75**, 034303 (2007).
[59] O. A. Rumyantsev and M. H. Urin, Phys. Lett. B **443**, 51 (1998).

[60] P. K. Raina, A. Shukla, S. Singh, P. K. Rath, and J. G. Hirsch, Eur. Phys. J. A **28**, 27 (2006).
[61] J. Barea, J. Kotila, and F. Iachello, Phys. Rev. C **91**, 034304 (2015).
[62] M. Horoi, Phys. Rev. C **87**, 014320 (2013).
[63] W. Satula, J. Dobaczewski, W. Nazarewicz, and M. Rafalski, Phys. Rev. Lett. **103**, 012502 (2009).
[64] F. Šimkovic, V. Rodin, and A. Faessler, Phys. Rev. C **87**, 045501 (2013).
[65] J. Suhonen, Nucl. Phys. A **853**, 36 (2011).
[66] J. Kotila and F. Iachello, Phys. Rev. C **85**, 034316 (2012).
[67] M. Doi, T. Kotani, H. Nishiura, and E. Takasugi, Prog. Theor. Phys. **69**, 602 (1983).
[68] P. Belli *et al.*, Phys. Rev. C **87**, 034607 (2013).
[69] E. Caurier, J. Menendez, F. Nowacki, and A. Poves, Phys. Rev. Lett. **100**, 052503 (2008).
[70] J. Menéndez, A. Poves, E. Caurier, and F. Nowacki, Nucl. Phys. A **818**, 139 (2009).
[71] E. Santopinto, H. García-Tecocoatzi, R. I. Magaña Vsevolodovna, and J. Ferretti (NUMEN Collaboration), Phys. Rev. C **98**, 061601 (2018).
[72] C. A. Bertulani, Nucl. Phys. A **554**, 493 (1993).